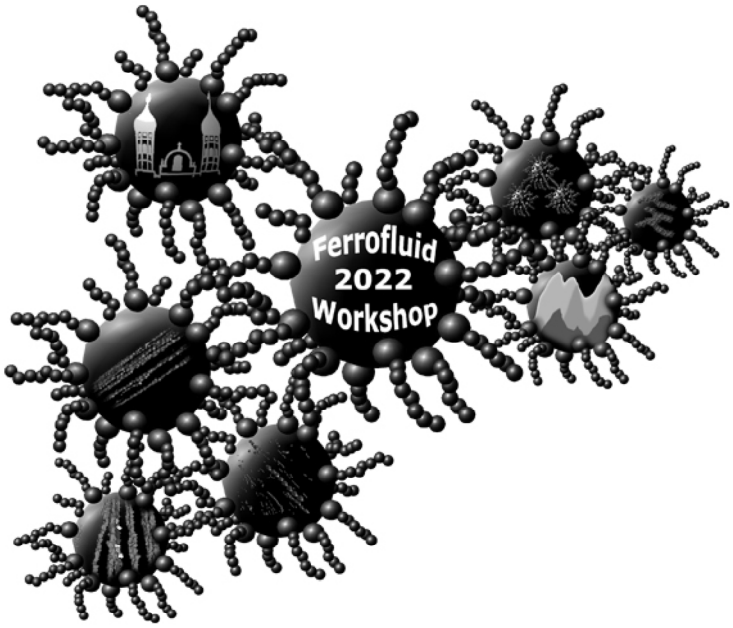

Benediktbeuern

September 28th - 30th 2022

Program Overview

Opening	28.09.2022	13:30 – 13:50
Experimental Methods		13:50 – 15:50
Coffee Break		15:50 – 16:30
Medical aplications and biotechnology		16:30 – 18:10
Postersession		18:10 – 20:00
Walking / Bus Tour	29.09.2022	08:45 – 16:00
Mountain Talks		
Winners of the Doctoral Thesis Award		17:00 – 18:30
Colloquium-Dinner		19:00 - … .
Synthesis	30.09.2022	09:00 – 10:00
Coffee Break		10:00 – 10:30
Theory, modelling and simulation		10:30 – 12:10
Closing		12:10 – 12:30

next trains to Munich will leave 13:04 and 13:58

Content

Program of the
19th German Ferrofluid Workshop

Benediktbeuern, September 28th – 30th 2022

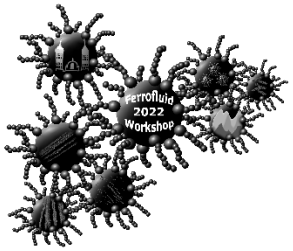

Wedensday, September 28th

13:30-13:50	***Opening***	
13:50	**Experimental methods**	
13:50-14:10	J. Kopp, J. Landers, S. Salamon, B. Rhein, S. Essig, R. Müller, S. Behrens, A. Schmidt, H. Wende	*Magnetic study of Bariumhexaferrite Nanoplatelets via Mössbauer Spectroscopy*
14:10-14:30	M. Küster, H. Nádasi, N. Sebástian, P. Hribar Boštjančič, D. Lisjak, A. Mertelj, A. Eremin, F. Ludwig	*Magnetic dynamics in suspensions of ferrimagnetic bariumhexaferrite nanoplatelets*
14:30-14:50	C. Czichy, S. Odenbach	*Influence of a mechanical stimulation on magnetic alginate hydrogel strands due to an external alternating magnetic field*
14:50-15:10	M. Kubík, Z. Strecker	*Response time of Magnetorheological Fluid on Rapid Change of Magnetic Field under Shear Loading*
15:10-15:30	M. Reiche, T. I. Becker, G. V. Stepanov, F. Becker, K. Zimmermann	Field-Controlled Bending of a Multipole Magnetoactive Elastomer for Vibration-Driven Locomotion
15:30-15:50	D. Kare Gowda, S. Odenbach	*Characterization of quasi-static mechanical properties of thermoplastic polyurethane magnetorheological elastomers*
15:50	***Coffee break & Posters***	

16:30	**Medical applications and biotechnology**	
16:30-16:50	S. Lyer, B. Friedrich, C. Janko, H. Unterweger, S. Cunningham, S. Dutz, H. Hackstein, R. Strauß, C. Bogdan, C. Alexiou, R. Tietze	*Peptide Functionalized SPIONs for the Acceleration of Sepsis-Diagnosis*
16:50-17:10	D. Eberbeck, M. Kruteva, L. Fruhner, A. Feoktystov, R. Thiermann, F. Wiekhorst	*Evaluation of the determination of the core-shell structure of magnetic nanoparticles*
17:10-17:30	D. Zahn, S. Jung, S. Pahlow, A. Stanca, J. Dellith, K. Saatchi, U. O. Häfeli, S. Dutz	*Adapting magnetic microspheres to medical applications*
17:30-17:50	F. Pfister, M. Kappes, B. Friedrich, C. Huber, R.P. Friedrich, R. Stein, C. Braun, S. Lyer, J. Band, E. Schreiber, C. Alexiou, C. Janko	*Targeted cell seeding of human vocal fold fibroblasts via superparamagnetic iron oxide nanoparticles*
17:50-18:10	F. Wolgast, T. Kahmann, E. Rösch, A. Lak, M. Schilling, F. Ludwig, T. Viereck	Low-cost standalone magnetic particle spectroscopy device for fast and sensitive immunoassays
18:10	***Posterssesion***	

Thursday, September 29th

approx. 08:30 Mountain and Alternative Tour

approx. 13:00 Mountain Talk

17:00 Winners of the Doctoral Thesis Award

19:00 ***Workshop dinner***

Friday, September 30th

9:00	**Synthesis**	
9:00-9:20	P. Jauch, J. Dietrich, N. Wilharm, C. Krömmelbein, F. Schütte, S. Riedel and S.G. Mayr	*Energetic electron assisted synthesis of bioderived ferrogels and smart hydrogels – fundamentals, applications, perspectives*
9:20-9:40	J. Landers, S. Salamon, R. Nadarajah, S. Tahir, B. Eggert, B. Gökce, H. Wende	*Towards FeRh-nanoparticle inks for printable magnetocaloric media*
9:40-10:00	M. Weißpflog, B. Hankiewicz	*Ferrite-based Magnetic Nanoparticles in a Smart Polymer Matrix*
10:00	***Coffee break & Posters***	
10:30	**Theory, modelling and simulation**	
10:30-10:50	G. J. L. Jäger, L. Fischer, T. Lutz, A. M. Menzel	*Tuning the thermal conductivity of magnetic gels and elastomers by external magnetic fields*
10:50-11:10	P. Gebhart, T. Wallmersperger	*A hybrid phenomenological model for hysteresis effects in isotropic magneto-active polymers at the macroscale level*
11:10-11:30	P. Kreissl, C. Holm, R. Weeber	*Studying the Interplay Between Steric and Hydrodynamic Interactions for Ellipsoidal Magnetic Nanoparticles in a Polymer Suspension*
11:30-11:50	A.A. Kuznetsov, V.S. Zverev, S.S. Kantorovich	*On a field-controlled mass transport in concentrated ferrofluids*
11:50-12:10	M. Biersack, A. Lakkis, O. Bilous, P. Sanchez, S. Kantorovich, R. Richter	*Coarsening Dynamics of Ferromagnetic Granular Networks under Impact of a Vertical Magnetic Field*
12:10	**Closing**	

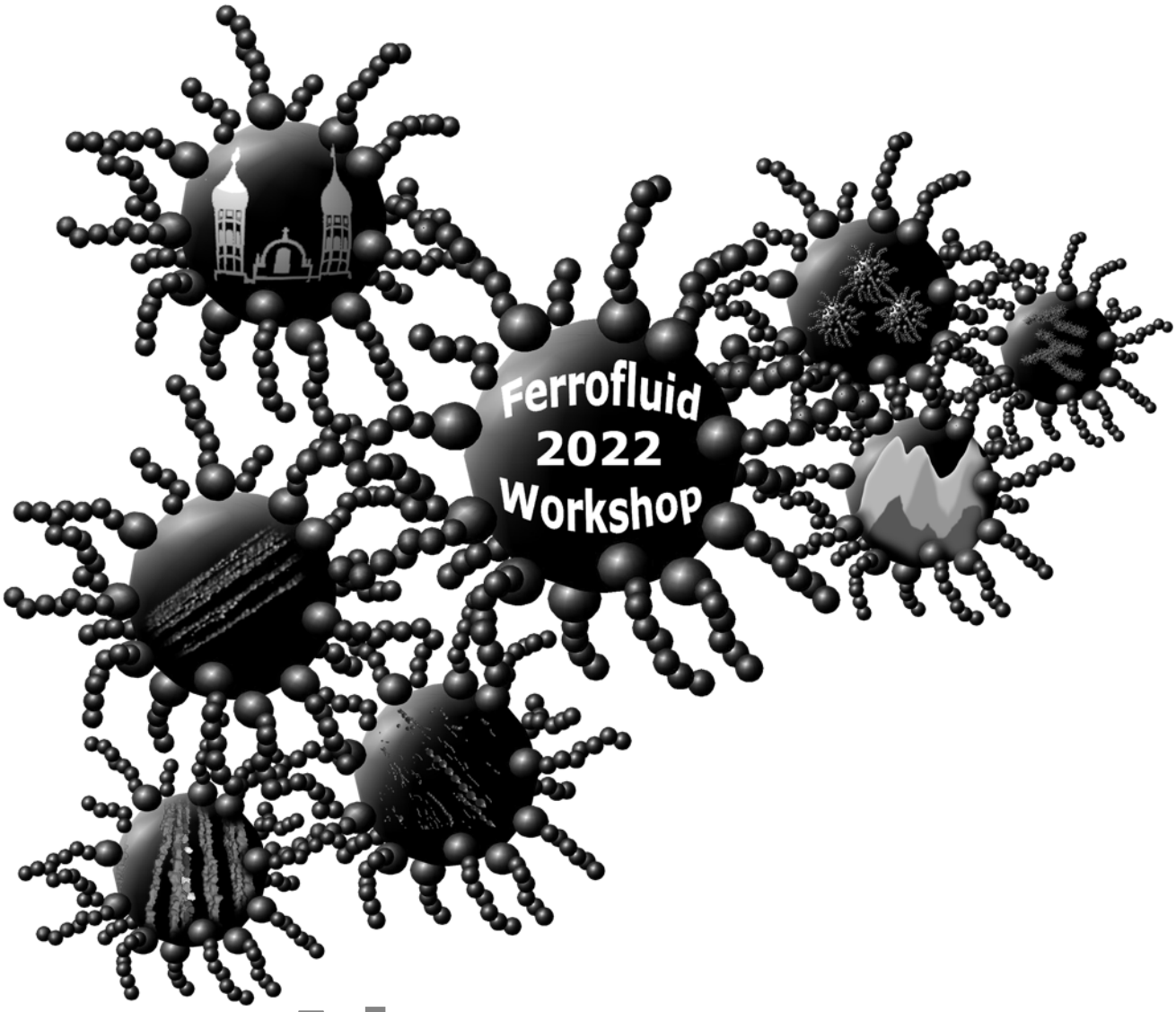

Abstracts

19th FERROFLUIDWORKSHOP

Abstracts

Ferrofluidic Couette flow in time-varying magnetic field

S. Altmeyer

Castelldefels School of Telecom and Aerospace Engineering, Universitat Politecnica de Catalunya, 08034 Barcelona, Spain

Despite time-dependent boundary conditions being ubiquitous in natural and industrial flows, to date the influence of such temporal modulations (e.g. with driving frequency Ω_H) has been given minor attention. The present problem addresses ferrofluidic Couette flow [1, 2] in between counter-rotating cylinders [3] in a spatially homogeneous magnetic field subject to time-periodic modulation. Such a modulation can lead to a significant inner Reynolds number Re enhancement [4] for both, either helical and toroidal flow structures.
Using a modified Niklas approximation [2, 5], the effect of low- and high- frequency modulation onto the primary instabilities, stability boundaries as well as on the non-linear oscillations that may occur is investigated. From this, we describe the system response on bistable co-existing solutions, around their stability thresholds to be sensitive to an alternating field until the appearance of intermittent behavior.

System setup

In the periodically modulated TCS, we give a sinusoidal modulation signal to the external magnetic field (parallel z-axis, uniform in space and harmonic in time) as $\mathbf{H}_z = [H_S + H_M \sin(\Omega_H t)]\mathbf{e}_z$. As earlier reported such a pure axial magnetic field *preserves* the system symmetries and only shift the stability thresholds [1, 6]. By using a modified Niklas approach [2, 1] the effect of the magnetic field and the magnetic properties of the ferrofluid on the velocity field can be characterized by the (time dependent) Niklas function [5]

$$s_z(t) = s_{z,S} + s_{z,M} \sin(\Omega_H t), \qquad (1)$$

with three control parameters, $s_{z,S}$ being the *static contribution*, $s_{z,M}$ the *modulation amplitude*, and Ω_H the *modulation frequency*.

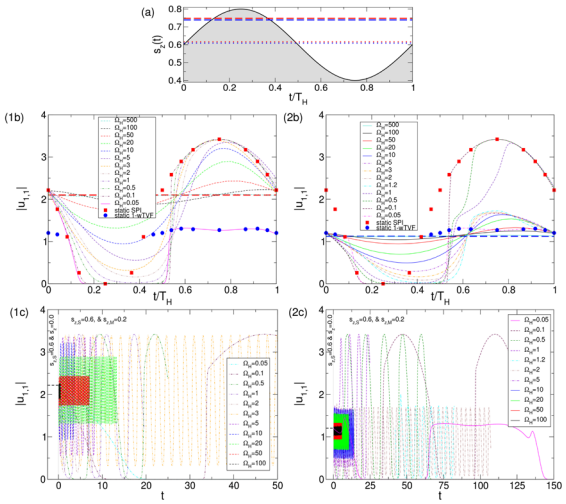

Figure 1: Non-linear system response across the instability. (a) Temporal oscillations of the control function $s_z(t)=s_{z;S}+s_{z;M}\sin(\Omega_H t)$ ($s_{z;S}=0.6$, $s_{z;M}=0.2$). (c) Time evolution of the dominant mode amplitude $|u_{1,1}|$ as a function of time for different driving frequencies Ω_H as indicated. The modulation $s_{z;M}$ starts at $t=0$, before only a static field $s_{z;S}=0.6$ ($s_{z;M}=0.0$) is present for (1) SPI and (2) wTVF, respectively. (b) Corresponding mode amplitudes $|u_{1,1}|$ as function of the reduced time $t=T_H$ ($T_H=2\Omega_H$ being the modulation period associated with the corresponding frequency). Red squares (■) and blue circles (•) in (b) show the stationary response to stationary magnetic field with magnetic field strength given by the actual value of $s_z(t)$.

Results

For parameters given in Fig. 1 the system becomes temporally subcritical for modulation amplitudes $s_{z,M}$ =0.2, while it *remains* supercritical in pure static case ($s_{z,M}$ =0.0) for (1) SPI and (2) wTVF, respectively. With decreasing driving frequency Ω_H the system response changes between subcritical CCF and supercritical wTVF for $1.1 \leq \Omega_H \leq 6.5$. Although the system response continuous to switch be-

tween supercritical and subcritical, for smaller values $0.1 \leq \Omega_H \leq 1.1$, the supercritical SPI appears, despite wTVF being the initial state. Regardless the initial state, wTVF or SPI, for the narrow region $0.06 \leq \Omega_H \leq 0.1$ *intermittent behavior* is found with ran dom exchange of wTVF or SPI as the appearing supercritical solution. Thereby both, the number of consecutive appearing same pattern (SPI or wTVF) and the number between switches from one to the other appear to be random. Further, for very low $\Omega_H \leq 0.06$ the system response is the same as seen before for SPI as initial condition. Thus the system is alternating between subcritical CCF and supercritical wTVF

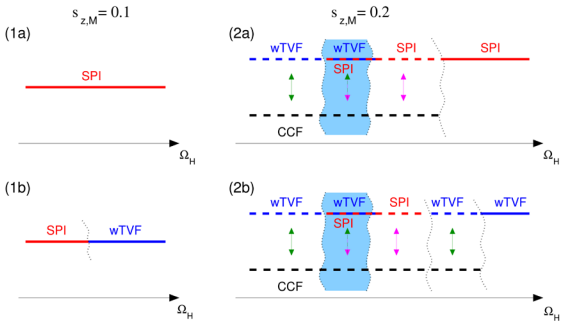

Figure 2: Schematic illustration for stability change/switch between di erent flow states, subcritical and supercritical dynamical system response, with variation in the driving frequency Ω_H (increasing left to right) for small (1) $s_{z;M}$=0.1 and large (2) $s_{z;M}$=0.2 modulation amplitude.

Conclusion

We found that the system response is selective to driving parameters across stability thresholds and instabilities. We detected that such an alternating field may provide a simple and accurate way to trigger the system response. As shown in the present work the flow can be controlled (i) between different supercritical flow solutions or (ii) between supercritical and subcritical flow solutions, which means to trigger either sub- or supercritical system response. General observation is that the high frequency limit (Fig. 2) results in a single supercritical solution, which is determined by the corresponding initial condition, either SPI or wTVF.

Acknowledgments

S. A. is a Serra Húnter Fellow.

References

[1] S. Altmeyer, C. Hoffmann, A. Leschhorn, and M. Lücke, Influence of homogeneous magnetic fields on the flow of a ferrofluid in the Taylor-Couette system. Phys. Rev. E 82, 016321 (2010).

[2] M. Niklas, Influence of magnetic fields on Taylor vortex formation in magnetic fluids. Z. Phys. B 68, 493 (1987).

[3] G. I. Taylor, Stability of a viscous liquid contained between two rotating cylinders. Philos. Trans. R. Soc. London A 223, 289 (1923).

[4] S. Altmeyer, On the ridge of instability in ferrofluidic Couette flow via alternating magnetic field. Scientific Reports 11, 4705 (2021).

[5] S. Altmeyer, Ferrofluidic Couette flow in time-varying magnetic field. J. Magn. Magn. Mater 552, 169205 (2022).

[6] M. Reindl and S. Odenbach, Effect of axial and transverse magnetic fields on the flow behavior of ferrofluids featuring different levels of interparticle interaction. Phys. Fluids 23, 093102 (2011).

Coarsening Dynamics of Ferromagnetic Granular Networks under Impact of a Vertical Magnetic Field

M. Biersack[1], A. Lakkis[1], O. Bilous[2,3], P. Sanchez[2], S. Kantorovich[2], R. Richter[1]

[1]*Experimentalphysik V, Universtät Bayreuth, 95440 Bayreuth (Germany)*
[2]*University of Vienna, Sensengasse 8, Vienna, 1090 Austria*
[3] *Faculty of Natural Sciences, National University of "Kyiv-Mohyla Academy", Kyiv, Ukraine*

Introduction

Magnetised steel spheres self-assemble due to anisotropic magnetic interactions. If one shakes a mixture of glass and steel beads with a supercritical vibration amplitude, inter-particle collisions hinder the aggregation and keep the mixture in a "gas phase" [1]. Below a critical vibration amplitude, magnetic forces lead, first, to the formation of individual chains and rings that merge into a network [2] as the system relaxes as shown in Fig. 1. If given enough time, the network eventually compacts into crystalline-like islands of magnetic beads.

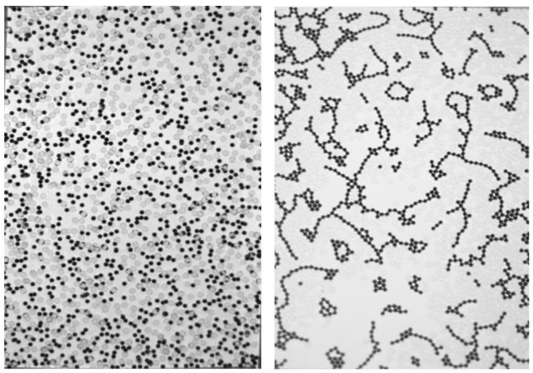

Figure 1 *Snapshot of the coarsening dynamics after a quench of the vibration amplitude from 3g to 1.93g. Gas phase (a) and transient networks (b). From [2].*

This scenario closely resembles the viscoelastic phase separation (VPS) introduced by Tanaka [3] for molecular mixtures. There phase separation arises from the different shear viscosities of both components, labelled as dynamic asymmetry by Tanaka. Also in our mixture magnetic forces rise the shear viscosity of the ferrogranulate in contrast to the glass phase. And indeed, in experiments and computer simulations we found first evidence that the coarsening dynamics can be describes as a VPS in the macroscale [3].
A homogeneous magnetic field oriented parallel to the system plane has been observed to "unknot" network structures orthogonal to the field [4]. In the following we focus on the impact of a homogeneous magnetic field oriented in vertical direction onto the VPS.

Experiment

A computer-controlled signal generator feeds a sinusoidal voltage signal into an amplifier which drives a vibration exciter. The vibrations are coupled via a long rod to the experimental vessel to avoid the magnetic stray field of the exciter. The vessel is filled with glass and steel beads. Pictures are recorded by means of a triggered camera. A Helmholtz-pair-of-coils serves to apply a vertical magnetic field.

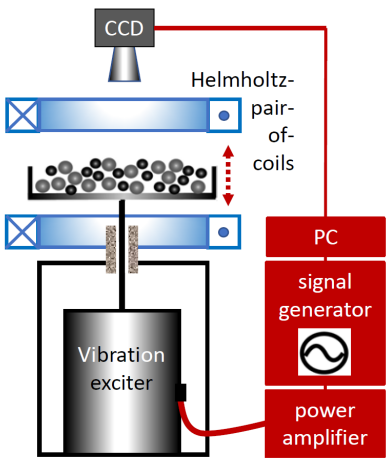

Figure 2. *Schematic of the experimental setup.*

Experimental Results

The mean degree of a node of the network has been proven to be a suitable order parameter [2]. It is plotted in Fig. 3. The upper most curve (B=0mT) shows a steep increase (chain formation) followed by a more gradual one, associated with the formation of networks [3]. With increasing values of the vertical induction B the growth of $\bar{k}$ is hampered.

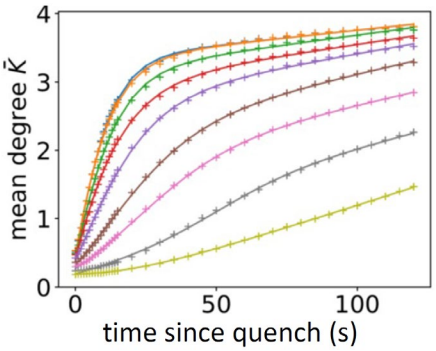

Figure 3. *Mean degree of a node vs time for different values of the applied vertical induction B, ranging from 0.0mT (blue, top) to 1.8mT (yellow, bottom). The lines indicate fits by a complemented logistic growth function.*

As displayed in Fig. 4 we observe a three-phase-state, namely mobile glass beads, the coarsening network, and a hexatic phase of isolated steel beads, indicating that B reduces the mobility of isolated steel beads, in this way hindering the growth of the networks.

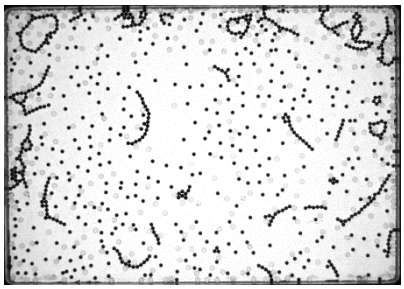

Figure 4. *Coexistence of networks and isolated beads at B=1.8mT, recorded 20s after the quench.*

Numerical Results

We study ferrogranulate via molecular dynamics simulations with a Langevin thermostat with a minimal coarse-grained model. In this model the spheres carry a magnetic point dipole in their centers. Our preliminary work [2,4] shows that to reproduce the susceptibility of the steel spheres it is sufficient as a first approach to introduce an additional central attraction (scaled by ε) between the steel spheres what we call here a Stockmayer Granulate. In simulations we treat the mechanical shaking as thermal fluctuations. The simulations are carried out with the package ESPResSO 4.1.4 [5].

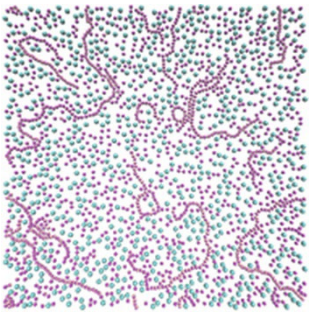

Figure 5. *Coexistence of networks and isolated beads for ε=0.5, H_z=1, recorded 2000 timesteps after the quench.*

Acknowledgments

The authors acknowledge financial support of the German-Austrian project "Coarsening dynamics of ferromagnetic granular networks – experiment and simulation" via Ri 1054/7-1 and I5160 FWF.

References

[1] D.L.Blair and A. Kudrolli, *Phys. Rev. E* 67 (2003) 021302.

[2] A. Kögel, P. Sanchez, R. Maretzki, T. Dumont, E. S. Pyanzina, S. S. Kantorovich, and R. Richter. *Soft Matter*, 14 (2018) 1001.

[3] H. Tanaka, *J. Phys: Condens. Matter* 12 (2000) R207.

[4] P. A. Sanchez, J. Miller, S. S. Kantorovich, R. Richter, *J. Magn. Magn. Mater*, 499 (2019) 166182.

[5] H. J. Limbach, A. Arnold, B. Mann, C. Holm, *Comput. Phys. Commun* 174 (2006) 704.

Influence of the measuring geometry surface on the stationary shear deformation of a structured magnetic fluid

D.Y. Borin, E.M. Spörl, S. Odenbach

Technische Universität Dresden, 01069 Dresden, Germany

Introduction

The study demonstrates a critical point concerning the influence of experimental conditions on the rheological response of a magnetic fluid. A suspension based on silicone oil and magnetic microparticles was pre-structured in an external homogeneous magnetic field and subjected to stationary shear using a rheometer in a plate-plate measuring geometry configuration. The type of measuring geometry surface and the concentration of magnetic particles in the suspension were varied to assess differences in the macroscopic response of the fluid.

Samples

In this study, suspensions based on silicone oil M10000 with a dynamic viscosity 10 Pa*s (GE Bayer Silicones, Germany) and carbonyl iron powder (CC grade, BASF, Germany) with an average particle size of about 5 μm were used. The highly viscous oil was chosen as a carrier liquid in order to counteract particle sedimentation, as no any special additives and stabilizers have been utilized. The magnetic powder was thoroughly mechanically mixed with the carrier medium in three volume concentrations (5, 25 and 40%). The resulting suspension samples were continuously stirred in external vessels to maintain their homogeneity.

Setup and method

Measurements were conducted using the Physica MCR 502 WESP rheometer (Anton Paar GmbH, Austria) equipped with the magnetorheological device MRD [1]. As measuring geometry a non-magnetic plate-plate arrangement was utilized, at that, as a rotor the Anton Paar PP20/MRD/TI geometry was used. This is a specially designed for MRD made of Ti plate having a working surface of 20 mm in diameter combined with an additional cover. The measuring configuration is shown schematically in Figure 1. The surfaces of the rotating plate (rotor) and the static plate were modified in two different ways. The first modification (Figure 2, left) is an abrasive paper with a medium grit of P400 and a thickness of ~0.5 mm. It is referred to as P400. The layer of the abrasive paper was replaced before each new measurement. The other modification used (Figure 2, right) is a foamed open pored material, hereinafter referred to as the anti-slip cover (ASC), with a layer thickness of 1 mm.

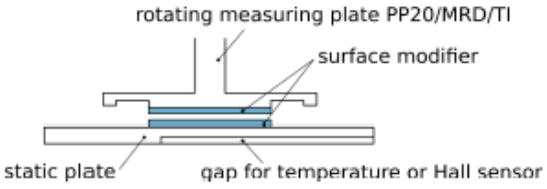

Figure 1. Schematic representation of the measuring configuration.

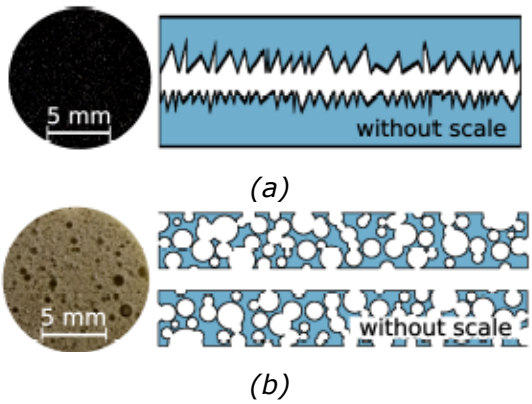

Figure 2. Photographic and schematic representation of the surface modifications of the measuring geometry: a - abrasive paper with a medium grit of P400; b - anti-slip cover made of a foamed open-pored material.

To evaluate a quasi-stationary shear deformation of the magnetic fluid, the sample was first structured, i.e. disposed under magnetic field influence, for at least 5 minutes. Then the specimen was loaded with a constantly increasing strain from0 to 10% and the corresponding shear stress on the moving rotor was measured.

Results and discussion

The response to the applied quasi-static shear of all the magnetic fluid samples tested in the reference measurements, without an applied field, was not systematically analyzed. In the zero field, the fluids behave like ordinary viscous bodies, which also does not induce significant shear stress as a result of quasi-static shear. The variation of shear stresses was in units of Pa and it was not possible to evaluate the in influence of different surfaces on the response of an unstructured fluid. The response to applied quasi-static shear of a field-structured fluid differs for both samples with different concentrations of magnetic particles and for different measuring geometry surfaces used. The exemplary results are shown in Figure 3. An influence of the surface modification on the shear stress development under the same operating conditions within quasi-static shear is to be clearly noted. In general, it is evident that changing the interaction conditions of the structured fluid with the surface of the measuring geometry dramatically affects the experimental observation result. The qualitative appearance of all the curves suggests that there could be a slippage of the particle structures over the geometry surfaces and/or particle structures are still not destroyed even at a maximum applied strain. The different results obtained for different suspension concentrations and magnetic field strengths can be explained by the fact that the morphology of the particle structure also differs in these cases. However, it is not possible to make precise and reliable statements about the actual behavior of the particle structures through these experiments. The critical relationship between the results obtained and the interaction of fluids of different compositions with different surface types is evident. Further details will be presented in the Workshop and are as well to be found in [2].

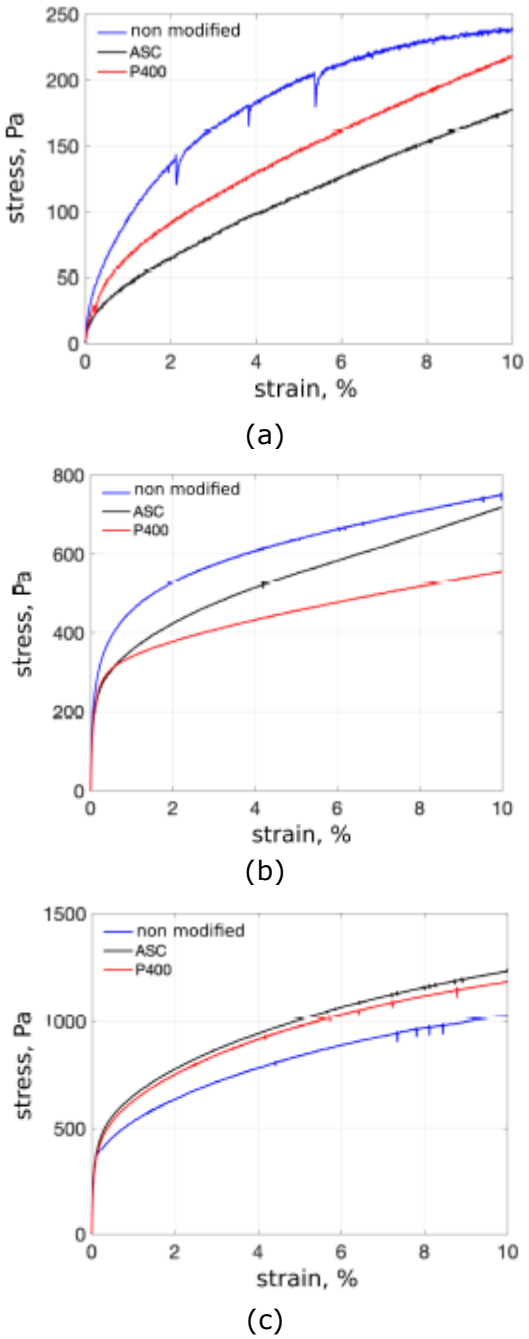

Figure 3. Strain-stress curves obtained *for the structured fluid with a) 5 vol.%, b) 25 vol. % and c) 40 vol. % at 100 kA/m.*

Acknowledgments

Financial support by Deutsche Forschungsgemeinschaft (DFG) under Grant Bo 3343/3-1 is gratefully acknowledged.

References

[1] J. Laeuger, K. Wollny, H. Stettin, S. Huck, Int. J. Mod. Phys. B 19, 1353-1359 (2005)

[2] D. Borin, E. Spörl, A. Zubarev, S. Odenbach, Eur. Phys. J. Spec. Top. 231, 1159–1163 (2022)

Influence of a mechanical stimulation on magnetic alginate hydrogel strands due to an external alternating magnetic field

Ch. Czichy, S. Odenbach

Chair of Magnetofluiddynamics, Measuring and Automation Technology, TU Dresden, 01069 Dresden, Germany

Introduction

Tissue Engineering (TE) is aiming to create patient specific implants through additive manufacturing to replace defect or destroyed tissue and restore its function. Therefore, scaffolds are generated, which are colonized with stem cells [1]. These cells can be animated e.g. through mechanical stimuli to differentiate and / or to multiply. A new approach for deforming the scaffolds is to apply an alternating magnetic field to a magnetic hydrogel as alginate-methylcellulose with magnetite [2].
The influence of a daily stimulation on the deformation behaviour and the particle structure was investigated in the presented study. Other considered parameters were the autoclaving of the matrix material and applying a stationary magnetic field with constant field gradient.

Materials and samples

The matrix consists mainly of a 3 wt% alginate dissolved in phosphate buffered saline (PBS).
Half of this solution is autoclaved at 121 °C for 20 min (high pressure, saturated steam, Systec D-23 tabletop autoclaves) since it is mandatory for the use of cells [1,2].
To increase the viscosity, 9 wt% methylcellulose is added, so that it can be used for extrusion printing in TE. As magnetic microparticles magnetite was chosen. The concentration in the samples was 25 wt%.
The samples were stored in cell culture medium for 14 days at 37 °C. The medium was renewed two times per week.
Half of the samples were stimulated using the bioreactor CyMAD [3]. The samples in question were exposed to an alternating field with a frequency of 1 Hz for 3 hours per day over a period of 14 days.

To analyse the influence of the stimulation and to determine the influence of autoclaved alginate-PBS-solution four groups were created, seen in Tab. 1.

Tab. 1: Parameter combinations used in this study

		autoclaved	
		yes	no
stimulated	yes	A_Stim	Norm_Stim
	no	A_CG	CG (control group)

Methods

In order to determine the deformation, an experimental setup was constructed using a Maxwell setup for a µCT, with which a constant magnetic field gradient could be applied.
µCT images were taken of the unloaded and the deformed state due to a magnetic field (MF). From these data, the position of the neutral fibre could be determined. The difference between the two states corresponds to the bending curve w. For the maximum deflection in the centre of the sample, the maximum elongation ε of the sample was determined.
3D-Images were also taken in the µCT using the experimental setup to analyse the particle structure. In this case, the samples were fixed so that no deformation could take place. First, a tomogram was taken without an applied MF. Then a MF was applied and after 30 min another measurement was carried out with the MF still applied.

Results and Conclusion

Fig. 1 shows the measured bending curves w and the elongation ε of the four parameter combinations mentioned in Tab. 1.

No significant differences can be identified between the 4 groups with regard to bending and elongation. This means that no material damage occurred due to the stimulation. Autoclaving, which destroys the chains, also has no discernible influence. Thus, it can be concluded that the network is stable. It is possible that the methylcellulose acts as a pseudo-cross-linker.

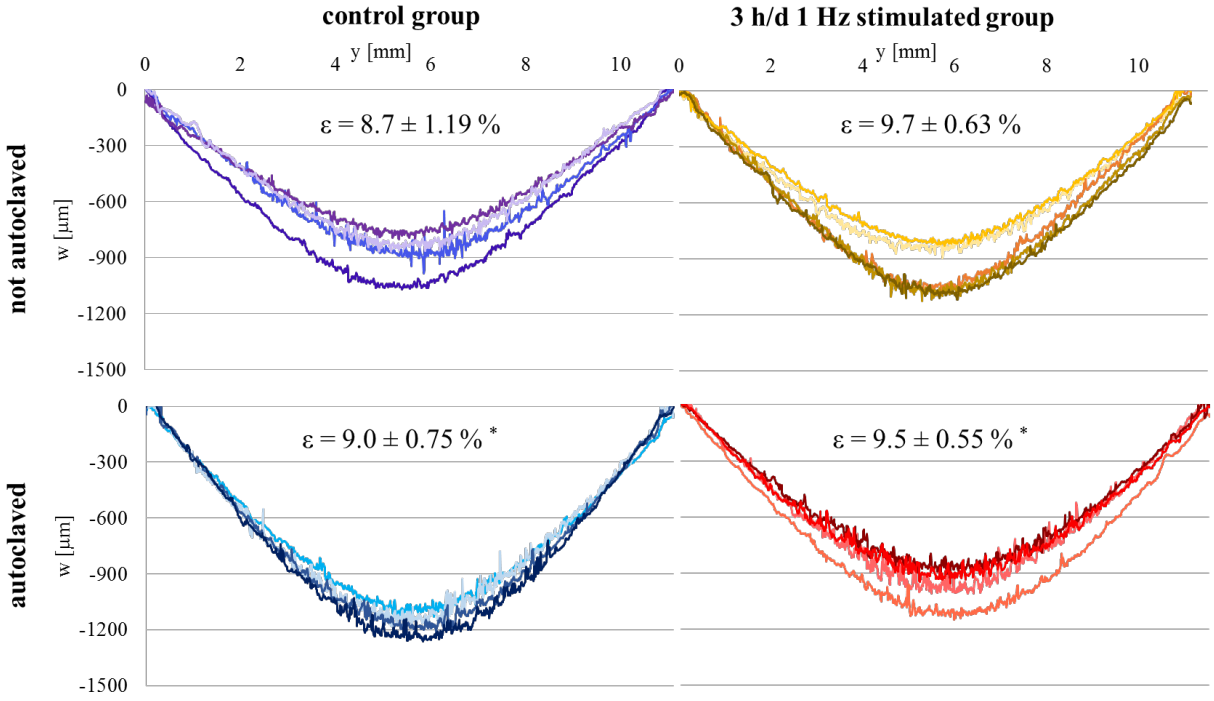

Fig. 1: Determined bending curves and the resulting mean values of the elongations of the four investigated parameter combinations (published in [3])*

Acknowledgments

The authors would like to thank the European Social Fund (ESF) and the Free State of Saxony for financial support of this project in the course of the ESF Young Researchers Group IndivImp at TU Dresden.

References

[1] Schütz, Placht, Paul, Brüggemeier, Gelinsky, Lode: „Three-dimensional plotting of a cell-laden alginate/methylcellulose blend: towards biofabrication of tissue engineering constructs with clinically relevant dimensions“ journal of tissue engegineering and regenerative medicine 11, p1574-1587, 2017, John Wiley & Sons, Ltd., https://doi.org/10.1002/term.2058

[2] Spangenberg, Kilian, Czichy, Ahlfeld, Lode, Günther, Odenbach, Gelinsky: Bioprinting of Magnetically Deformable Scaffolds”, ACS Biomater. Sci. Eng 2, p648-662, 2021, https://dx.doi.org/10.1021/acsbiomaterials.0c01371

[3] Czichy; Kilian, Wang, Günther, Lode, Gelinsky, Odenbach: “CyMAD bioreactor: a cyclic magnetic actuation device for magnetically 1 mediated mechanical stimulation of 3D bioprinted hydrogel scaffolds” Journal of the mechanical behaviour of biomedical materials, 2022, 131, 105253, https://doi.org/10.1016/j.jmbbm.2022.105253

Evaluation of the determination of the core-shell structure of magnetic nanoparticles

D. Eberbeck[1], M. Kruteva[2], L. Fruhner[2], A. Feoktystov[3], R. Thiermann[4], F. Wiekhorst[1]

[1] *Physikalisch-Technische Bundesanstalt, Berlin, Germany*
[2] *Forschungszentrum Jülich GmbH, JCNS-1 & IBI-8, 52425 Jülich, Germany*
[3] *Forschungszentrum Jülich GmbH, Jülich Centre for Neutron Science JCNS at Heinz Maier-Leibnitz Zentrum MLZ, 85748 Garching, Germany*
[4] *Fraunhofer-Institut für Mikrotechnik und Mikrosysteme IMM, Mainz, Germany*

The type and quality of coating crucially determine the behaviour of magnetic nanoparticles (MNP) within biological applications. For example, the half-life period of MNP receiving a second PEGylation during synthesis could be enhanced from minutes to about 1 hour [1]. The opsonisation of magnetic nanoparticles (MNP) by biomolecules turned out to be important within this context. For example, nanoparticles opsonised by the abundance of clustering proteins exhibit a reduced cellular uptake (stealth effect) [2]. While charge and density directly affect the opsonization of the MNP by biomolecules, the thickness affects the aggregation behaviour via modulation of the dipole-dipole interaction.

Hence, beyond the right core sizes of MNP for a biological application, also charge, thickness and density of the coating should be known. These quantities should be measured within the body fluid of interest because the structure of the coating may depend on the medium. Integral magnetic measurement of MNP motility might have a great potential for the estimation of the coating parameters.

Within this work we estimated the thickness δ_s and the density ϕ_s of the coating of MNP applying quasistatic field dependent magnetisation (M(H)) and alternating current susceptibility (ACS) together with Transmission Electron Microscopy (TEM), Small Angle X-ray and Neutron Scattering (SAXS, SANS). SANS represents the gold standard among the integral methods for the estimation of δ_s and ϕ_s. In this way, the core-shell structure of MNP in organic dispersion medium and of aqueous dispersions of rather small size (mean diameter $d \leq 20\,\mathrm{nm}$) can be successfully determined [3]. However, in medical applications like Hyperthermia and MPI, hydrophilic MNP with a well-defined large core diameter ($d = 25 \ldots 30\,\mathrm{nm}$) are required. As model systems for the determination of the core shell structure we used three different SHP samples (Ocean Nanotech, USA) because of its very narrow core size distribution ($\sigma \leq 0.1$) and well-defined coating. Although the nominal structure of these MNP appears to be well describable by the spherical core-shell model, our previous investigations showed that a successful fit to all data required the introduction of so-called WMA (weak magnetic areas within the cores) and small clusters of MNP which were roughly approximated by modified spherical particles. Now, these clusters will be replaced by dimers and trimers composed of ellipsoids of revolution (Figure 1).

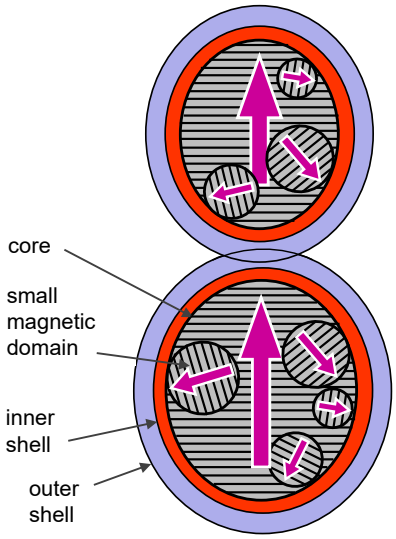

***Figure 1**: Model of core-shell MNP and dimers of MNP (differing in size) with intercalated or squeezed outer shells. WMA were phenomenologically modelled by non-interacting small magnetic domains.*

Beyond the core size distribution, δ_s and ϕ_s the ellipsoid parameter, ε_c, the volume fractions of WMA, ϕ_{m2}, dimers and trimers, ϕ_{DT}, relative trimers, $\phi_{T,r}$, trimers which become transformed to dimers in ACS, ϕ_{T2D}, the fraction of cluster forming monomers which are connected along z-direction, ϕ_{ctz}, the compression factor for the shell, k_δ, were introduced. This reduced residual systematic deviations significantly. The omission of these single parameters deviated other parameters from its best fit value and it enhanced systematic deviations of the fit (Table 1).

Table 1: Obtained values of new fit parameters ("full model") and the exemplary effect of its removal on the dispersion of the core size distribution, σ_c, and on the increment of systematic deviation of the fit from the data of the most susceptible method.

parameter change	σ_c incr.	method	incr.
full model	0.085(1)		
ϕ_{m2}=0.51(2) → 0	-2(4)%	M(H)	13 %
ϕ_{DT}=0.59(2) → 0	-50(6)%	SAXS	31 %
$\phi_{T,r}$=0.81(7) → 0	-4(3)%	SAXS	8 %
ϕ_{T2D}=0.65(3) → 0	3(2)%	SAXS	9 %
k_δ=0.22(3) → 1	-6(2)%	SAXS	2 %
ε_c=1.22(1) → 1	16(2)%	TEM	20 %
ϕ_{ctz}=0.36(4) → 1	14(2)%	TEM	28 %

The fit of the model to all data sets yields the thickness and the density of the total coating layer with an uncertainty below 5% when SANS-data were included (Table 2). Without SANS-data the uncertainty may strongly increase depending on the match of the model. For SHP-30 the model with 2 shells with fixed values for the inner hydrophobic shell, $\delta_{s,1} = 2.5\,\mathrm{nm}$, $\phi_{s,1} = 1$, yields $\delta_{s,2} = 1.9(2)\,\mathrm{nm}$ and $\phi_{s,2} = 0.39(6)$. The total thickness exceeds the nominal value of $\delta_s = 2.6\,\mathrm{nm} \ldots 3\,\mathrm{nm}$. That might be attributed to, e.g., an incomplete attachment of the second coating layer. Note, in SANS residual systematic deviations are still present, notably for SHP-30B (Fig. 2). This hints to larger inhomogeneities within the coating of SHP-30B which experience a much stronger opsonisation than SHP-30.

Table 2: Thickness δ_s and density ϕ_s of the total coating layer applying the data of all methods and all without SANS.

sample	$\bar{d}_c$ nm all	δ_s nm all	ϕ_s all	δ_s nm all-SANS	ϕ_s all-SANS
SHP-25	22.0(1)	-	-	4(2)	-
SHP-30	28.6(1)	3.9(1)	0.81(2)	4.1(2)	1.0(3)
SHP-30B	26.9(1)	4.8(2)	0.46(2)	3(2)	1(1)

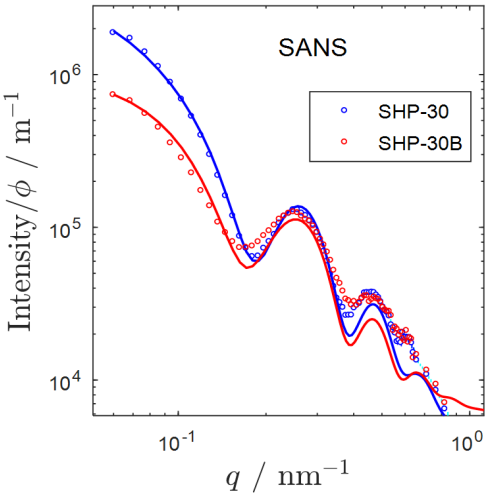

***Figure 2**: SANS-data and best fit curves of SHP-30 and SHP-30B, normalised to the volume fraction of core particles.*

We have shown that the thickness of the coating layer can be estimated reliably for ellipsoidal particles with dimers and trimers fitting a comprehensive model to multiple data sets even without harnessing SANS. Applying SANS data, more details of the shell and its density could be resolved. Furthermore, the details found for the core structure and moments could be used as inputs for microscopic modelling of magneto-mechanical behaviour of real samples.

Acknowledgments

This work was supported by the DFG priority program 1681.

References

[1] H. Kratz, et al., Nanomaterials **9**, (2019).
[2] S. Schöttler, et al., Nat. Nanotechnol. (2016).
[3] M. V. Avdeev and V. L. Aksenov, Uspekhi Fiz. Nauk (2010).

A hybrid phenomenological model for hysteresis effects in isotropic magneto-active polymers at the macroscale level

Philipp Gebhart, Thomas Wallmersperger

Institute of Solid Mechanics, Technische Universität Dresden, 01062 Dresden, Germany

In recent years there has been an increasing interest in the theoretical and experimental study of field responsive, functional composite materials. Magnetoactive polymers (MAPs) are a special class of field responsive solids that comprise of a polymeric matrix with dispersed micro-sized magnetizable particles. Based on the magnetic properties of the underlying ferromagnetic filler particles, MAP composites can be classified into two categories: (i) soft and (ii) hard MAPs. Soft MAPs comprising magnetically soft particles, e.g. carbonyl iron, exhibit negligible hysteresis loss and demagnetize completely after the removal of the external magnetic field which in consequence leads to reversible deformation mechanisms. In contrast, Nd- FeB particle-filled hard MAPs exhibit distinct nonlinear, dissipative material behavior, such as the characteristic magnetic and ”butterfly” field-induced strain hysteresis. In the present work, we present a comprehensive variational modeling framework for hard MAPs including the response of the soft MAPs as a limiting case.

We outline ingredients of the constitutive theory based on the framework of generalized standard materials, that necessitates suitable definitions of the total energy density function and the dissipation potential. Key idea of the constitutive approach is an additive split of the material part of the total energy density function into three contributions associated with (i) an elastic ground-stress, (ii) the magnetization and (iii) a magnetically induced mechanical stress, respectively [1, 2]. We propose suitable constitutive functions

in an energy-based setting that allow to reproduce magnetic and butterfly hysteresis along with their rate-independency.

The performance of the developed variational modeling framework is demonstrated by solving some application-oriented boundary value problems. The main emphasis of the numerical studies lies on the investigation of the magnetostrictive effect of hard MAPs at the macroscale level as well as on the in depth analysis of pre-magnetized beam structures undergoing large deformations.

Acknowledgments

This research has been financially supported by the Deutsche Forschungsgemeinschaft in the framework of the Priority Programme SPP1681.

References

[1] P. Gebhart and T. Wallmersperger, A constitutive macroscale model for compressible magnetoactive polymers based on computational homogenization data: Part I - Magnetic linear regime, IJSS, 236-237, 111294, 2022.

[2] P. Gebhart and T. Wallmersperger, A constitutive macroscale model for compressible magnetoactive polymers based on computational homogenization data: Part II - Magnetic nonlinear regime, IJSS, 2022, submitted.

Size-dependent Diffusion Behaviour of Magnetic Probe Particles in Complex Fluids

M. Hess

In many biological or material systems, the mutual interdiffusion and interaction of nanoscopic building blocks plays a crucial role. To investigate the flow behavior of microstructured materials on the micro- or nanoscale with spatial resolution, an increasing number of methods have been developed. When the size of the probe particles is in the same range as the characteristic length scales within the material, deviations from the rheological performance, as obtained by conventional methods, are expected. In this work, nanorheological experiments on different polymer model systems using the method of Magnetic Particle Nanorheology (MPN) are performed under systematic variation of the tracer size.

For this purpose, magnetically blocked $CoFe_2O_4$ nanoparticles of variable hydrodynamic size with narrow size distribution are synthesized and characterized, whereby the size of the particles is adjusted by coating with a SiO2 shell. The tracer particles are used to extract frequency-dependent rheological properties such as storage G' and loss G'' modulus, viscosity η, relaxation time τ, rotational diffusion coefficient D_τ and scaling relations, among others.

A spectrum of polymeric model materials are investigated ranging from linear poly(ethylene glycol) (PEG) aqueous solutions over covalently crosslinked polyacrylamide hydrogels (PAMH) to functionalized star-shaped PEG molecules with moieties able to form dynamic networks in the presence of metal ions.

Different size relation regimes of the structural units within the sample to tracer particle size are obtained from MPN for the different polymeric systems. For the PEG solutions, the correlation depends on the polymer volume fraction and molar mass of the polymer. If the hydrodynamic particle size is below the radius of gyration, R_g, three different time regimes are accesible, depending on the relationship between the correlation length ξ, the tube diameter a and the hydrodynamic particle diameter d_h. If covalently crosslinked networks are investigated by doping with tracer particles embedded in the meshes, the nanorheological results clearly depend on the relation of tracer particle size to mesh size. There is a sharp transition when the mesh size of the gel equals the hydrodynamic diameter d_h of the tracers. For the star-PEG dynamic networks, a mesh size close to the expected value of an ideal network, as well as close to the particle size is found. This allows the probe particle to detect local dynamic processes like for example the breaking of the metal-ligand bond.

The results provide substantial insight into the structural and dynamic behavior of the investigated polymer systems by analyzing the diffusion properties of probe particles of variable hydrodynamic size.

Tuning the thermal conductivity of magnetic gels and elastomers by external magnetic fields

G. J. L. Jäger, L. Fischer, T. Lutz, A. M. Menzel

Institut für Physik, Otto-von-Guericke-Universität Magdeburg, Universitätsplatz 2, 39106 Magdeburg, Germany

Motivation

Over the past few decades, a significant amount of research has been dedicated to the mechanical properties of magnetic gels and elastomers that can be tuned from outside by external magnetic fields [1]. Most prominently, this concerns the magnetorheological effect, that is, magnetically induced changes in stiffness and damping behavior [2]. Additionally, magnetostrictive behavior in terms
of magnetically induced changes in shape were addressed [3].
It has been demonstrated that these changes in behavior are correlated with magnetically induced internal restructuring of the magnetizable inclusions [4]. Specifically, the reversible formation of chain-like aggregates can be achieved, against the restoring elastic counterforces arising from the necessary elastic deformations of the surrounding medium [5, 6].
When this internal restructuring occurs, it is conceivable that also the transport properties through the materials are affected. Nevertheless, this aspect has only rarely been addressed. Few studies are available concerning electric conductivity [7], and even less concerning thermal conductivity [8]. Furthermore, many corresponding works compare the conductivities of finalized materials in which anisotropic structures have been imprinted by applying external magnetic fields during synthesis. Here, we address the magnetic tunability of the thermal conductivity of magnetic gels and elastomers by magnetically induced internal restructuring [9].

Theoretical description

We approach the topic using established bead-spring modeling of magnetic hybrid materials [10]. To this end, magnetizable beads are assigned to randomly selected nodes of randomized hexagonal spring lattices. Upon magnetization, new arrangements are found by numerical forward integration in time.
The overall thermal conductivities of the systems are determined by applying two different constant temperatures to two opposite sides such that magnetization and overall temperature gradient are parallel. We then solve the discretized heat equation under these given boundary conditions. For this purpose, a Voronoi tesselation scheme in combination with a cellular model are employed. Beads that are in virtual contact are basically treated as one object concerning thermal conductivity. This allows us to address larger systems at the cost of not resolving individual magnetizable particles. So far, our evaluations address flat thin sheets or membranes of magnetic gels and elastomers.

Results

Indeed, our description reproduces the internal restructuring upon magnetization. On average, larger induced magnetic moments and larger numbers of magnetizable particles lead to more pronounced chain formation. As a consequence, the overall thermal conductivity rises. The opposite applies when we increase the mean particle distance, which leads to less pronounced chain formation and reduced thermal conductivity. We have not found any obvious dependence on the aspect ratio of the investigated systems. Interestingly, the behavior can be nonmonotonic for selected individual systems. That is, we increase the initially induced magnetic moment, but the overall thermal conductivity decreases. It turns out that the origin of this apparent discrepancy is kinetic. Stronger magnetic interactions lead to quicker dynamics and faster motion of individual magnetized

beads. As a consequence, the inner parts of the chain-like aggregates form quicker. However, this accelerated process is too fast for the previous outer parts of the chains to follow and they cannot catch up, which leaves them behind. In this way, an increase in magnetization can counteract the formation of long chains.
Briefly, we also consider the process of switching off the magnetization. We find that the separation and reorganization into the initial state occurs much quicker than the formation of the aggregates. Each inclusion then is driven by the elastic restoring forces individually. The dynamics of each inclusion does not need to rely on collective magnetic interactions with other inclusions, after these interactions have been amplified by preceding formation of shorter aggregates.

Conclusions

We have demonstrated by our study that magnetic gels and elastomers indeed have the potential to serve as magnetically tunable soft switches for adjusted thermal conductivity. Similar reasoning should apply to electric conduction.
Specifically, we hope to stimulate by our work experimental investigations on the effect, but also analyses based on quantitative, largerscale simulation approaches. Obvious future tasks are to find realizations to maximize the effect while minimizing the associated amplitudes of the necessary magnetic fields.

Acknowledgments

We thank the German Research Foundation (DFG) for support through the SPP 1681 via grant no. ME 3571/3-3 (G.J.L.J., L.F.), through the research grant no. ME 3571/5-1 (T.L.), and through the Heisenberg grant no. ME 3571/4-1 (A.M.M.).

References

[1] S. Odenbach, Arch. Appl. Mech. **86**, 269 (2016).
[2] M. R. Jolly, J. D. Carlson, B. C. Muñoz, T. A. Bullions, J. Intel. Mater. Syst. Struct. **7**, 613 (1996).
[3] L. Fischer, A. M. Menzel, J. Chem. Phys. **151**, 114906 (2019).
[4] M. Schümann, S. Odenbach, J. Magn. Magn. Mater. **441**, 88 (2017).
[5] T. Gundermann, P. Cremer, H. Löwen, A. M. Menzel, S. Odenbach, Smart Mater. Struct. **26**, 045012 (2017).
[6] M. Puljiz, S. Huang, K. A. Kalina, J. Nowak, S. Odenbach, M. Kästner, G.
[7] K. Auernhammer, A. M. Menzel, Soft Matter **14**, 6809 (2018).
[8] J. L. Mietta, P. I. Tamborenea, R. M. Negri, Soft Matter **12**, 6430 (2016).
[9] D. Diaz-Bleis, C. Vales-Pinzón, Y. Freile-Pelegr´ın, J. J. Alvarado-Gil, Carbohyd. Polym. **99**, 84 (2014).
[10] G. J. L. Jäger, L. Fischer, T. Lutz, A.
[11] M. Menzel, submitted (2022).
[12] G. Pessot, M. Schümann, T. Gundermann, S. Odenbach, H. Löwen, A. M. Menzel, J. Phys.: Condens. Matter **30**, 125101 (2018).

Energetic electron assisted synthesis of bio-derived ferrogels and smart hydrogels – fundamentals, applications, perspectives

Philine Jauch, Johannes Dietrich, Nils Wilharm, Catharina Krömmelbein, Friedrich Schütte, Stefanie Riedel, Stefan G. Mayr

Division of Biocompatible and Bioactive Surfaces, Leibniz-Institute for Surface Modifiation, Leipzig / Division of Surface Physics, Department of Physics and Earth Sciences, University of Leipzig, email: stefan.mayr@iom-leipzig.de

Energetic electron beams constitute a highly versatile tool for tailoring biomaterials properties of bioderived hydrogels with high spatial resolution. Based on electron-induced hydrolysis, reactions, ranging from crosslinking, chain scission and functionalization to arrest of magnetic nanoparticles, can be induced without the need for adding additional - potentially hazardous – reagents. This allows for synthesis of highly bioactive switchable composites, in particular ferrogels, stimuli responsive gels as well as shape memory gels. Within this presentation we will first review the fundamentals of energetic electron assisted hydrogel modification, regarding particularly the reaction kinetics in collagen. We will then focus on applying these finding for tailored hydrogel modification towards stimuli responsive gels, in particular ferrogels. This includes a collagen-based ferrogel actuator with reversible peak strains as large as 150%. We will also discuss application within the field of biomedicine, that are currently being developed, as well as future visions in an outlook.

Funding by the DFG – SPP 1681 (MA 2432/6) is gratefully acknowledged.

Characterization of quasi-static mechanical properties of thermoplastic polyurethane magnetorheological elastomers

D. Kare Gowda, S. Odenbach

Chair of Magnetofluiddynamics, Measuring and Automation Technology, TU Dresden, 01069 Dresden, Germany

Introduction

Magnetorheological elastomers (MREs) are elastomer composites embedded with magnetic particles, which belong to the group of smart materials with a rapid response to stimulation by an external magnetic field. Thermoplastic MREs can be stimulated by both temperature and magnetic field. In recent times, thermoplastic polyurethane magnetorheological elastomers (TPU-MREs) have gained significant interest among researchers due to its multi stimulated compliance with superior mechanical properties, ease of preparation and wide range of applicability [1,2]. The change in moduli of an MRE with respect to an applied external magnetic field provides the information on the sensitivity of the MRE and is termed as magnetorheological effect (MR effect). In this work we have presented the temperature dependence of MR effect of TPU-MRE.

Materials and methods

Isotropic TPU-MRE samples were prepared from a two component TPU system. PU 450 and PH 330 from Elantas were mixed with plasticizer Dimethyl Phalate from Sigma-Aldrich and Höganas ASC 200 iron particles of size 30 to 80 µm. The composition of the investigated samples contained 40 wt.% of iron particles within the TPU matrix material, containing 40.9 wt.% of PU 450, 13.1 wt.% of PH 330 and 6 wt.% of the plasticizer.
Isotropic cylindrical rod-shaped samples were post cured at 100 °C for 24 hours before testing. New methods of testing the MRE samples presented in Borin et.al. [3] was implemented to obtain more reliable results. Quasistatic tensile and torsion tests were conducted using a modified HAAKE MARS III rheometer, schematic representation in figure 1.

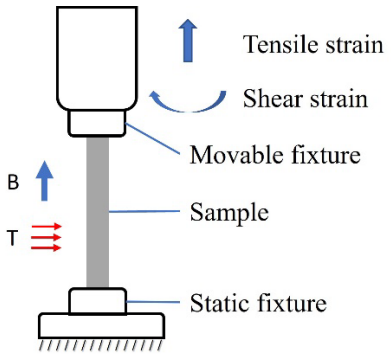

Figure 1: Schematic representation of the test setup B is magnetic field direction and T is external heating.

All the tests were conducted at three different temperatures with and without the presence of a magnetic field of 250 mT. As the quasistatic tensile and torsion tests were conducted within the linear elastic limit of the sample, the slopes of the corresponding stress-strain curves provide the values of the Young's modulus (*E*) and the shear modulus (*G*). Table 1 shows the sequence in which the samples were tested.

Table 1; Test sequence of quasistatic tensile (Te.) and torsion (To.) of the sample.

Temp.	23 °C		40 °C		60 °C	
Test	Te.	To.	Te.	To.	Te.	To.
0 mT	1	3	5	7	9	11
250 mT	2	4	6	8	10	12

If the TPU-MRE sample is assumed to be a perfectly incompressible isotropic material and Poisson's ratio ν is 0.5 under the quasistatic test conditions. The relation between the moduli *E* and *G* should be agreeable according to the equation,

$$E = 2(1 + \nu)G \qquad (1)$$

with E being three times G.

Results and Discussion

From figure 2, the results indicate that both the Young's and the shear modulus of the TPU-MRE sample decrease with the increase in temperature. As the composition of the TPU had a relatively very low amount of hardener, it results in the formation of a phase separated microstructure with high soft segment content in the TPU matrix. With the increase in temperature, the bonding force between the soft and hard segments reduces, leading to higher freedom of movement for soft segment [4]. This results in the decrease in the moduli with the increase in temperature.

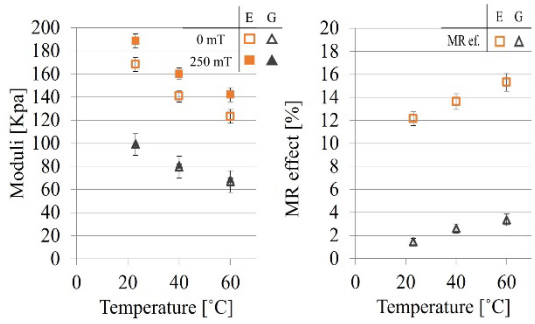

Figure 2: The measured Young's modulus (E) and shear modulus (G) of the sample (Left) and the corresponding MR effect (right).

According to the equation (1) the values of the ratio between the Young's and shear modulus of the TPU-MRE, at all the corresponding test conditions are within 2. Hence the TPU-MRE doesn't agree with the conditions of a perfectly incompressible isotropic material. This might be due to the morphological complexity of the TPU matrix and its interaction with the iron particles [2,4].

The increase of the MR effect with the increasing temperature shown in figure 2 indicates that, the reduction in stiffness of the TPU-MRE at higher temperature has resulted in increase in MR effect. Regarding the difference in the MR effect between the tensile test and the torsion test, the direction of magnetic field plays a major role. As shown in figure 1, in the case of tensile test, the magnetic field direction is along the direction of the strain and perpendicular in the case of torsion test. The inter particle force of attraction is higher along the magnetic field direction. Hence the resistance to deformation experienced by the TPU-MRE in presence of magnetic field is more in tensile test than in torsion test. Regarding the repeatability of the results, the samples were tested twice after the first test cycle and the results vary within 5 %.

Acknowledgments

The authors would like to express their thanks to the Deutsche Forschungsgemeinschaft (DFG) for financial support within the SPP2100 research program (OD 18/28-1).

References

[1] Bastola, A. K., Paudel, M., Li, L., and Li, W., "Recent progress of magnetorheological elastomers: a review," *Smart Materials and Structures*, Vol. 29, No. 12, 1 Jan. 2020, p. 123002. doi: 10.1088/1361-665X/abbc77.

[2] Zhang, G., Zhang, Z., Sun, M., Yu, Y., Wang, J., et al., "The Influence of the Temperature on the Dynamic Behaviors of Magnetorheological Gel," *Advanced Engineering Materials*, 1 Jan. 2022, p. 2101680. doi: 10.1002/adem.202101680.

[3] Borin, D., Kolsch, N., Stepanov, G., and Odenbach, S., "On the oscillating shear rheometry of magnetorheological elastomers," *Rheologica Acta*, Vol. 57, No. 3, 1 Jan. 2018, pp. 217–227. doi: 10.1007/s00397-018-1071-2.

[4] Son, T. W., Lee, D. W., and Lim, S. K., "Thermal and Phase Behavior of Polyurethane Based on Chain Extender, 2,2-Bis-[4-(2-hydroxyethoxy)phenyl]propane," *Polymer Journal*, Vol. 31, No. 7, 1 Jan. 1999, pp. 563–568. doi: 10.1295/polymj.31.563.

Ferronematic phases with strong coupling behavior based on liquid crystalline polymer decorated nanoparticles

K. Koch

Department Chemie, Institut für Physikalische Chemie, Universität zu Köln, Greinstr.4-6, D-50939 Köln

The combination of magnetic nanoparticles and liquid crystalline (LC) phases leads to materials with unique magneto-optic behavior induced by a coupling between the magnetic director of the particles and the nematic director of the LC host. [1] The strength of this coupling strongly depends on the stability of the particles against agglomeration, which is still the biggest challenge for the synthesis of stable ferronematic phases. [2]
In this work, novel ferronematics are synthesized and fully characterized. Therefore, strategies for the compatibilization of nanoparticles with LC phases are developed in order to obtain stable ferronematic phases. For this purpose, nanoparticles are surface-functionalized with polymer brushes using a *grafting-from* process and a *grafting-to* process. For the grafting-from process, a novel route for the surface modification of nanoparticles with poly(dimethylsiloxane) (PDMS) brushes by surface-initiated ring-opening polymerization of cyclosiloxanes catalyzed by strong phosphazene bases and initiated by particle surface-attached hydroxyl groups is developed.

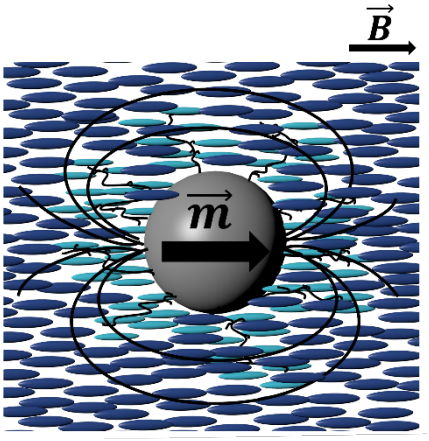

Figure 1. Scheme of LC polymer brush particle.

In the *grafting-to* process, side-chain liquid crystalline polysiloxane brushes are synthesized separately and then grafted covalently to the surface of nanoparticles of different magnetic behaviors. The functionalized particles are used as doping agents for the LC host 4-cyano-4'-pentylbiphenyl (5CB) in order to synthesize stable ferronematic phases. The impact of the different particles on the properties of the LC phase is systematically analyzed with respect to the dopant concentration. Furthermore, the magneto-optic behavior is investigated in magnetic field-dependent capacitance measurements.

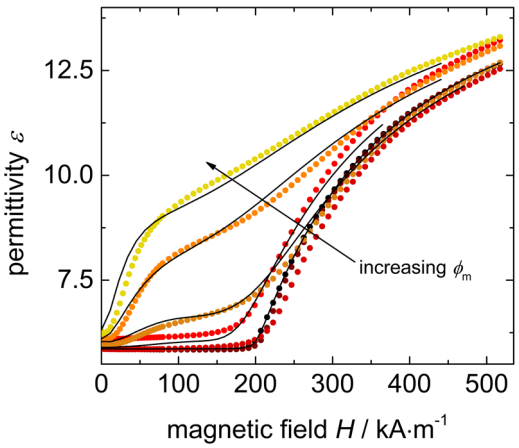

Figure 2 Capacitance measurements with parallel B and E field for pure 5CB(black) and 5CB doped with 9OCB-PHMS@$CoFe_2O_4$ and in volume fractions from 0.01 vol% up to 0.5 vol%.

In summary, the results of this thesis give important insights for the compatibilization of nanoparticles with LC phases and the production of stable ferronematics and contributes to a better understanding of the magneto-nematic coupling in the novel materials.

Acknowledgments

Financial support is acknowledged from DFG-SPP 1681 "Feldgesteuerte Partikel-Matrix-Wechselwirkungen" (SCHM1747/10). K. K. acknowledges support by the International Helmholtz Research School of Biophysics and Soft Matter (IHRS BioSoft).

References

[1] F. Brochard, P. G. de Gennes, *J. Phys.* **1970**, *31*, 691–708.

[2] O. Buluy, S. Nepijko, V. Reshetnyak, E. Ouskova, V. Zadorozhnii, A. Leonhardt, M. Ritschel, G. Schönhense, Y. Reznikov, *Soft Matter* **2011**, *7*, 644–649.

Magnetic study of Bariumhexaferrite Nanoplatelets via Mössbauer Spectroscopy

J. Kopp[1], J. Landers[1], S. Salamon[1], B. Rhein[4], S. Essig[3], R. Müller[2], S, Behrens[3], A. Schmidt[4], H. Wende[1]

[1] *Faculty of Physics and Center for Nanointegration Duisburg-Essen (CENIDE), University of Duisburg-Essen*
[2] *Leibniz Institute of Photonic Technology, Jena*
[3] *Institute of Catalysis Research and Technology (IKFT), Karlsruhe Institute of Technology*
[4] *Institute for Physical Chemistry, University of Cologne*

Liquid crystalline (LC) systems have a wide range of applications as they combine the properties of a liquid and orientability in electric fields. In turn, if magnetic nanoparticles are added in such systems, we obtain magneto-responsive liquid crystals. Barium ferrite (BaM) platelets with their relatively high coercivity and their anisotropic shape can be considered as a promising type of nanoparticles for use in such magneto-responsive LC systems.

Accordingly, this work is geared towards the magnetic characterization of different anisotropic barium ferrite nanoplatelets using magnetic field and temperature dependent Mössbauer spectroscopy as well as magnetometry.

BaM nanoplatelets used for our study were synthesized using different methods such as the glass crystallization method [1] and hydrothermally based on the works of M. Drofenik et al [2, 3]. Within the relatively complex hexagonal magnetoplumbite structure, the iron atoms are located on 5 different lattice positions (octahedral 12k, 4f1, 2a, tetrahedral and bipyramidal 2b sites), with ferrimagnetic ordering and some peculiar magnetic properties. To study these in detail we apply Mössbauer spectroscopy in combination with magnetometry experiments.

Spectra of samples prepared by the glass crystallization method show bulk-like structure with clearly distinguishable sublattice contributions (fig. 1). In contrast, in nanoplatelets prepared hydrothermally, subspectral contributions overlap with each other, to an extent depending on the synthesis parameters. This could indicate altered iron environments, presumably due to limited thickness of the platelets, resulting in a high fraction of surface atoms and potentially some atomic disorder.

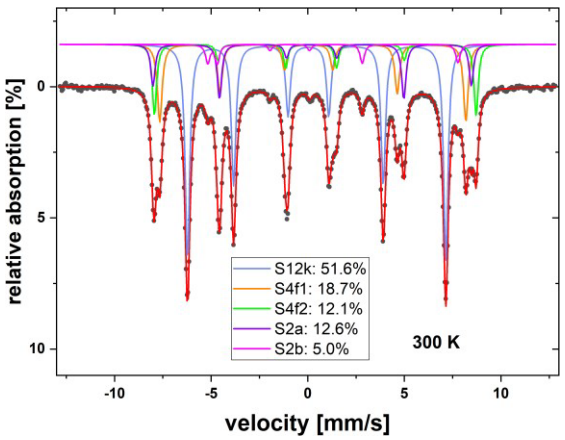

Fig 1: Mössbauer spectrum of BaM nanoplatelets synthesized by the glass crystallization method, showing 5 sextet subspectra, each representing one lattice position.

Especially information about the small contribution of the 2b-site is mainly lost due to the spectral overlap. Literature suggests that using higher temperatures during the hydrothermal synthesis process, leads to higher nanoplatelet thickness with more bulk-like structure [4], which is also indicated in our temperature dependent Mössbauer studies.

Furthermore, field dependent Mössbauer experiments were performed to analyze the particles' alignment behavior, showing magnetic orientation at ca. 1T (fig. 2). Based on the line ratios of the individual Mössbauer lines, an almost complete reorientation of the particles can be seen at ca. 5 T. Likewise, from the effective hyperfine fields the alignment of coaxial ferrimagnetic moments can be resolved for each sublattice contribution individually.

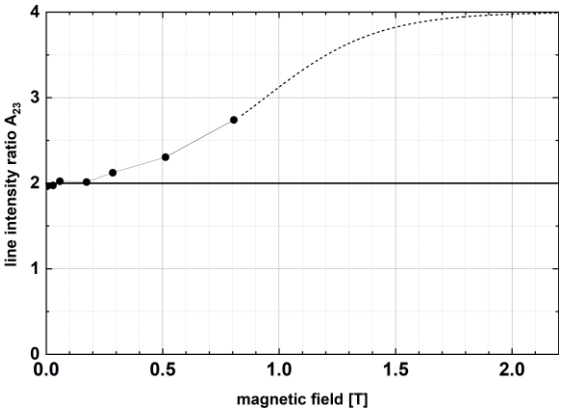

Fig. 2: Line intensity ratio A23 indicative for the degree of the magnetic alignment, where A23=4 corresponds to complete orientation along field direction. Dashed line is a guide-to-the-eye.

Outlook

The current study is focused on the magnetic characterization of Barium ferrite powder samples. The next step is to use functionalized BaM nanoplatelets in liquid crystalline systems and study their orientational behavior via different external stimuli. First attempts to stabilize and characterize the platelets in LC-based media are undergoing.

Acknowledgments

We gratefully acknowledge funding by the DFG through LA5175/1-1.

References

[1] B.T. Shirk, W.R. Buessem, *Magnetic properties of barium ferrite formed by crystallization of a glass.* **Journal of the American Ceramic Society**. 53 (1970), 192–196

[2] M. Drofenik, M. Kristl, A. Žnidaršič, D. Hanžel, D. Lisjak, *Hydrothermal Synthesis of Ba-Hexaferrite* Nanoparticles, **Journal of the American Ceramic Society**, 90 (2007) 2057- 2061

[3] M. Drofenik, i. Ban, G. Ferk, D. Makovec, A. Znidarsic, Z. Jaglicic and D. Lisjak, *The Concept of a Low-Temperature Synthesis for Superparamagnetic BaFe12O19 Particles,* **Journal of the American Ceramic Society** , vol. 93, no. 6, pp. 1602-1602, 2010.

[4] D. Makovec, B. Belec, T. Goršak, D. Lisjak, M. Komelj, G. Dražić and S. Gyergyek *Discrete evolution of the crystal structure during the growth of Ba-hexaferrite nanoplatelets***, Nanoscale, The Royal Society of Chemistry ,** vol. 10, 30 (2018), pp. 14480-14491

Studying the Interplay Between Steric and Hydrodynamic Interactions for Ellipsoidal Magnetic Nanoparticles in a Polymer Suspension

Patrick Kreissl, Christian Holm, Rudolf Weeber

Institute for Computational Physics, University of Stuttgart, Allmandring 3, 70569 Stuttgart, Germany

In soft magnetic systems consisting of magnetic nanoparticles in a polymeric environment, interesting properties can arise from the coupling of the particles' magnetic to the viscoelastic properties of their surroundings. We recently showed that hydrodynamics are an important coupling mechanism for spherical nanoparticles in polymeric environments and can lead to experimentally observed shifts in the AC susceptibility spectra [1, 2]. However, when considering non-spherical particles, such as nickle nanorods or hematite spindles, additional coupling by steric interactions is expected. Our focus is therefore to study the interplay between steric and hydrodynamic interactions using molecular dynamics simulations.

Simulation Model

A bead–spring representation is used for the polymers, where monomers are connected with harmonic springs and a purely repulsive (WCA) potential is used to account for excluded volume interactions. For hydrodynamics the efficient lattice-Boltzmann algorithm is used. The ellipsoidal magnetic particles are represented as 'raspberries', consisting of homogeneously distributed fluid coupling points to achieve proper fluid coupling of the particle as a whole. An example for the ellipsoids used is shown in fig. 1.

Rotational Friction Factors

AC susceptometry is a common tool to asses the magnetical properties of composite magnetic systems experimentally. In the linear- response regime the susceptibility χ as a function of frequency f shows a Debye-like form

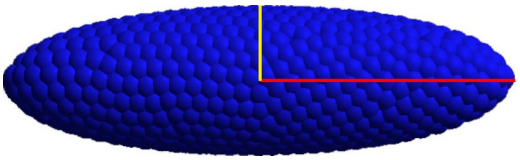

Figure 1: Snapshot of an ellipsoidal raspberry particle with axial ratio $p = l_{ax}/l_{eq} = 4$ (equatorial semiaxis $l_{eq} = 3$ [x], indicated yellow; axial semiaxis $l_{ax} = 12$ [x], drawn red).

$$\chi(f) = \frac{\chi_0}{1 + if\tau} \qquad (1)$$

where χ_0 is the zero-frequency susceptibility and τ the characteristic decay time of the magnetic moment. Higher decay times shift the position of the Debye loss-peak to lower frequencies. As we consider magnetically blocked particles, the decay time is determined by the friction hindering rotational reorientation of the magnetic particle (and its magnetic moment) through Brownian motion. For ellipsoidal particles the decay time will be different depending on the orientation of the magnetic moment within the particle. We consider the cases of the magnetic moment being co-aligned with the long axial semiaxis and with an equatorial short semiaxis, respectively.

In our simulations, we obtain rotational friction factors $\Gamma_{ax;eq}$ through measuring the rotational diffusivity via the Green-Kubo relation to the autocorrelation function of the angular velocities $\omega_{ax,eq}$,

$$D^{rot}_{ax,eq} = \int_0^\infty < \omega_{ax,eq}(t)\,\omega_{ax,eq}(0) > dt \qquad (2)$$

The friction factors are obtained by subsequent use of the Einstein relation

$$\Gamma_{ax,eq} = \frac{k_B T}{D^{rot}_{ax,eq}\,\Gamma_{Stokes}} \qquad (3)$$

where Γ_{Stokes} is the Stokes-friction of a sphere with equivalent volume as the respective ellipsoid. The friction factor thus indicates a lower ($\Gamma_{ax;eq}<1$), equal ($\Gamma_{ax;eq}=1$) or higher ($\Gamma_{ax;eq}>1$) friction than the equiv alent Stokes-sphere. In a Newtonian fluid, for equatorially aligned mag-

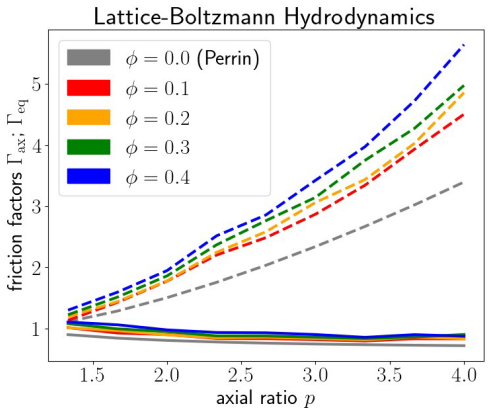

Figure 2: Friction factors of ellipsoidal magnetic nanoparticles with explicit hydro- dynamic coupling to surrounding polymers at different polymer volume fractions φ for various axial ratios p. Dashed lines correspond to axial moments, solid lines to equatorial moments.

netic moments the friction is slightly decreased whereas there is a significant increase for axial magnetic moments (gray curve, fig. 2). When polymers are added, equatorial moments see a marginal increase of the friction factor. Contrary, there is a significant effect on the relaxation of axial moments. There are monotonous friction increases with both larger polymer volume fraction and axial ratio of the ellipsoids.

For reference, Langevin simulations are run, replicating the dynamics of the ellipsoids and polymers, but without hydrodynamic coupling. As shown in fig. 3, the relaxation of equatorial moments is basically unaffected by purely steric interactions with surrounding polymers. For axial moments, larger friction factors are observed with increasing anisotropy of the particles and polymer concentration. The overall increase, however, is much lower than with hydrodynamics considered.

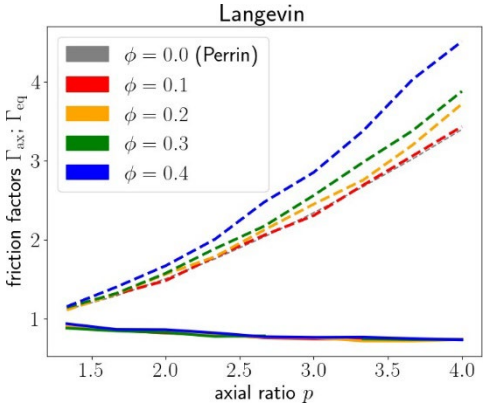

Figure 3: Friction factors obtained from Langevin simulations (no hydrodynamics).

Our simulations assert that for ellipsoidal particles with axial magnetic moments, increasing polymer concentrations lead to monotonously larger friction factors. Steric interactions are more appreciable and the friction significantly increased when hydrodynamic coupling is included. Somewhat surprisingly, however, there is basically no effect of steric interactions on the relaxation of equatorial magnetic moments and even with hydrodynamic interactions it is almost negligibly small.

References

[1] P. Kreissl, C. Holm and R. Weeber, Soft Matter 17, 147–183, 2021.

[2] E. Roeben, L. Roeder, S. Teusch, M. Effertz, U. K. Deiters and A. M. Schmidt, Colloid Polym. Sci. 292, 20132023, 2014.

Response time of Magnetorheological Fluid on Rapid Change of Magnetic Field under Shear Loading

M. Kubík, Z. Strecker

Brno University of Technology, Faculty of Mechanical Engineering, Technická 2, Brno, Czechia

Introduction

The transient behaviour (transient response) of MR actuators is an important parameter for modern suspension systems working with real-time control. The response time of the actuator on the control signal is a key factor. The currently published designs of MR actuators achieved great transient behaviour (response time roughly 1.2 ms). It can be stated that the response time of MR fluid itself is probably close to the response time of the MR actuators.

The MR fluid response time is composed of other partial time responses which are differently important depending on the operating conditions and the method of MR fluid loading. The response time of MR fluid can be divided into (i) hydrodynamic response time, (ii) particle structure development response time, and (iii) rheological response time. The rheological response time is connected with the structuring particle's time and the development of shear stress in MR fluid during the deformation (flow). Laun and Gabriel [1] experimentally determined the rheological response time of MR fluid as 2.8 ms. They used sinusoidal excitation and the determined time lag between magnetic flux density and shear stress. Koyanagi et al. [2] developed a method for a measurement the response time of ER fluid. This team experimentally determined the response time as 0.95 ms.

The information about the transient behaviour of MR fluid is limited. The main aim of this paper is to experimentally determine the rheological response time of MR fluid under shear loading.

Materials and methods

The unique design of the rheometer, which allows measuring rheological response time, is presented. This design allows rapid change of magnetic field due to suitable selected material of magnetic circuit (SMC) and fast current controller. The experimental test rig is composed of an electric motor with encoder, developed rheometer, load inertia, lever, and force sensor, see Figure below.

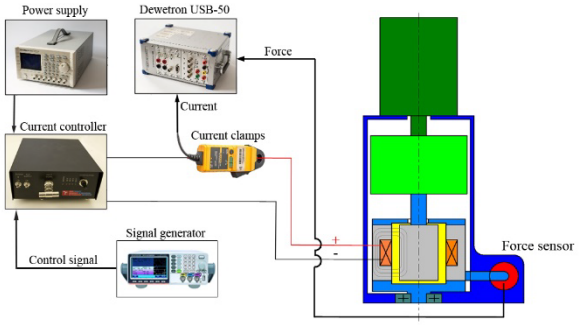

Figure 1 *Experimental test rig and measuring chain [3].*

The aim of the experiments was to determine shear stress in MR fluid and magnetic field over time. The shear stress was measured indirectly (calculated) based on data from the MEG20 force sensor. The magnetic field in the gap corresponds with the electric current course and was measured by Fluke i30 current clamps. These two signals were recorded and conditioned with a sampling frequency of 200 kHz by the Dewetron USB-50 analyzer. The measurement procedure was as follows: (i) 10 s measurement without magnetic field, and (ii) 10 s measurement with the application of the magnetic field. This procedure was necessary for the elimination of non-constant friction forces in the rheometer and viscous forces. It was necessary to determine the transfer function between the measured magnetic field and shear stress in MR fluid.

Results

Figure 2 shows the effect of shear rate on the course of shear stress (in the time domain). With the increasing shear rates, the response time decreases. An initial

dead time of 0.4 ms can also be seen, which is independent of the shear rate level. The previous study measured a dead time of 0.6 ms for MR fluid, which is consistent with our experiments. We assume that the measured dead time of 0.4 ms is related to the chaining of ferromagnetic particles (microstructure formation) in the MR fluid.

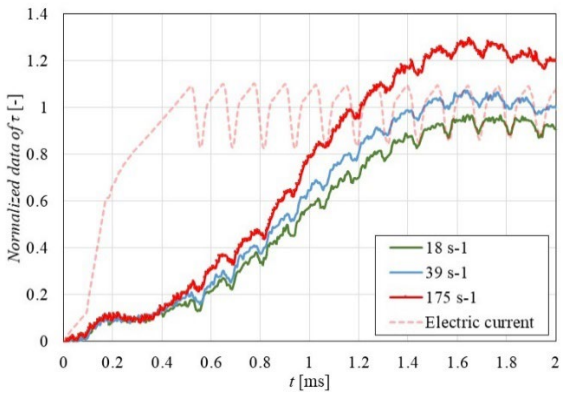

Figure 2 *Effect of shear rate on the course of shear stress [3].*

The rheological response times shown in figure 3 were determined from the experimental data and evaluated from the transfer function for four different MR fluids.

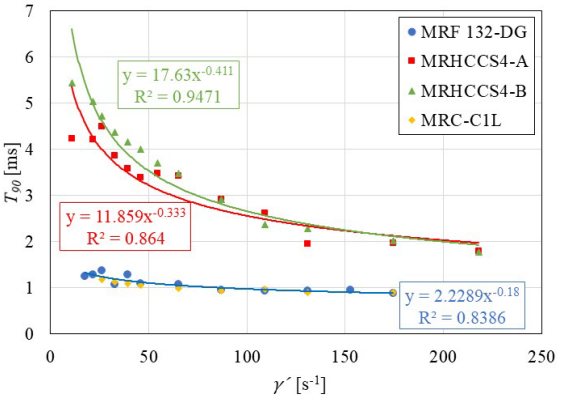

Figure 3 *Effect of shear rate on rheological response time [3].*

The higher the shear rate, the shorter the rheological response time. The response time ranges from 5.5 ms to 1.9 ms for the shear rate range of 11 - 218 s^{-1} for fluids MRHCCS4-A and MRHCCS4-B. MRF 132-DG and MRC-C1L fluids exhibit a shorter response time than other fluids in the range from 1.4 to 0.8 ms. Those fluids exhibit approximately 2.8 times lower carrier fluid viscosity than the carrier fluid of MRHCCS4-A and MRHCCS4-B. MR fluid response time data was generalized using non-dimensional response time T* and Mason number M_n, see figure 4. The one master curve was determined by curve fitting from measured data, see red line. This is an important conclusion because the master curve allows the determination of rheological response time for a given MR fluid and given load.

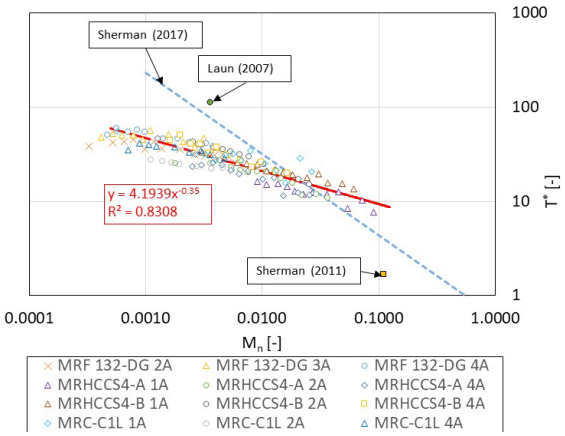

Figure 4 Measured data in the non-dimensional form [3]

Conclusion

This paper deals with the experimental determination of the magnetorheological fluid transient response (rheological response time) on the rapid change of a magnetic field in shear load mode. The one master curve was determined from measured data.

Acknowledgments

This paper and experiments have been made possible thanks to the Czech Science Foundation (GAČR) within the scope of the project No. 20-23261Y.

References

[1] Laun H M and Gabriel C 2007 Measurement modes of the response time of a magneto-rheological fluid (MRF) for changing magnetic flux density Rheol. Acta 46 665–76

[2] Koyanagi K and Terada T 2010 Time Response Model of ER Fluids for Precision Control of Motors J. Intell. Mater. Syst. Struct. 21 1517–22

[3] Kubík M, Válek J, Žáček J, Jeniš F, Borin D, Strecker Z and Mazůrek I 2022 Transient response of magnetorheological fluid on rapid change of magnetic field in shear mode Sci. Rep. 12 10612

Magnetic dynamics in suspensions of ferrimagnetic bariumhexaferrite nanoplatelets

Melvin Küster[1], Hajnalka Nádasi[2], Nerea Sebástian[3], Patricija Hribar Boštjančič[3], Darja Lisjak[3], Alenka Mertelj[3], Alexey Eremin[2], Frank Ludwig[1]

[1] *Institut für Elektrische Messtechnik und Grundlagen der Elektrotechnik und LENA, TU Braunschweig, Braunschweig, Germany*
[2] *Institut für Physik, ANP, Otto-von-Guericke-Universität Magdeburg, Magdeburg, Germany*
[3] *J. Stefan Institut, Ljubljana, Slovenia*

Introduction

Stable colloidal suspensions of nanoparticles offer an exciting opportunity to mimic molecular materials and explore their structural and dynamic properties. Recent research has shown that dense dispersions of hexagonal barium hexaferrite nanoplatelets coated with an ionic surfactant form a nematic phase even in an isotropic solvent such as n-butanol [1,2]. The combination of strong magnetic correlations and the orientational order results in the stabilization of a ferromagnetic state [3].
Here, we report the study of magnetization dynamics and the magnetomechanical effect of a colloidal dispersion of barium hexaferrite nanoplatelets in rotating and oscillating magnetic fields. In particular, we address the effect of magnetic and electrostatic interactions.

Experiment

Scandium-doped barium hexaferrite (BaHF) nanoplatelets with DBSA surfactant [1] were suspended in isotropic 1-butanol with concentrations between 7.5 mg/mL and 304 mg/mL. The magnetic moments of these nanoplatelets are directed perpendicularly to their basal planes. The sample with the highest BaHF nanoplatelet concentration (304 mg/mL) exhibits nematic order. To vary the strength of electrostatic interactions, different concentrations of DBSA surfactant were prepared.
The dynamics of the BaHF platelets is studied using AC susceptometry in a frequency range from 0.1 Hz – 9 kHz and for field amplitudes up to 5 mT. The fluxgate-based setup also allows measurements in rotation magnetic fields and ACS measurements in superimposed static fields either parallel or perpendicular to the sensing AC field [4]. The magnetomechanical effect is studied in a spherical cavity suspended on a torsional balance for field amplitudes up to 0.5 mT.

Results

Fig. 1 depicts the ACS spectra measured in the most diluted BaHF suspension for a fixed ratio between nanoplatelet and DBSA concentration of 87:13. For all AC field amplitudes a single peak in the spectrum of the ACS imaginary part is discernable, which shifts with increasing field amplitude towards lower frequencies. For other ratios c_{MP}/c_{DBSA}, several relaxations modes were observed even at such low c_{MP} [5]. This underlines the importance of properly adjusting the ratio between magnetic and electrostatic interactions.
Fitting the characteristic frequency, determined from the peak position in the χ'' spectra in Fig. 1, as a function of field amplitude with the model by Yoshida and Enpuku [6] we estimated a magnetic moment of $m = 4.3 \cdot 10^{-18}$ Am^2, in fair agreement with the value estimated from static magnetization measurements. Thus, this mode is attributed to the relaxation of individual nano-platelets.
The comparison of the normalized ACS spectrum with the torsional balance spectrum – both measured at 0.5 mT – show that they perfectly match in agreement with the model by Torres-Diaz and Rinaldi [7], which proposes that the torque density N_V is given by

$$N_V \propto H_0^2 \chi''$$

with magnetic field amplitude H_0. The conversion efficiency of the magnetic torque into the mechanical is particularly strongly pronounced in our system since the Néel relaxation mechanism is suppressed. The origin of the magnetomechanical torque is the vortex flow sustained by rotating MNPs.

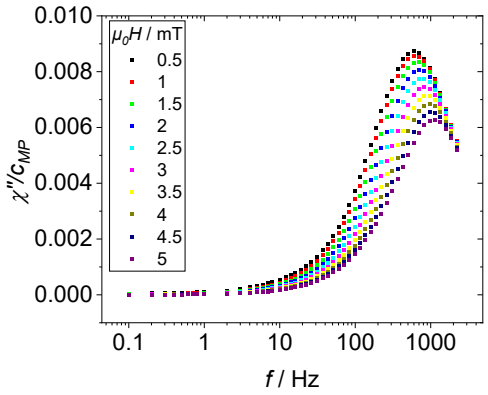

Fig. 1: Spectra of the normalized ACS imaginary part χ'' for the suspension with c_{MP} = 7.5 mg/ml and a ratio c_{MP}/c_{DBSA} = 87:13.

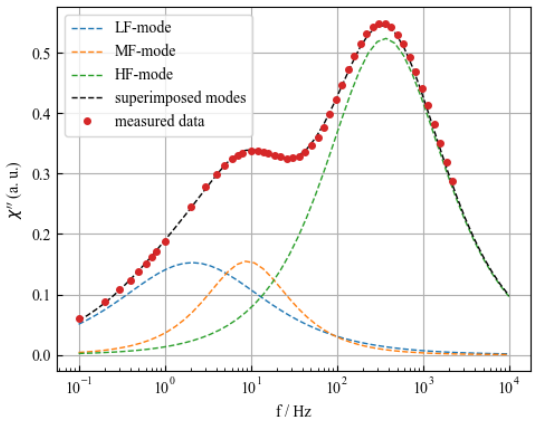

Fig. 2: Spectrum of the ACS imaginary part χ'' and its presentation by three relaxation modes.

For higher nanoplatelet concentrations, up to three relaxation modes are observed (Fig. 2), even for a ratio c_{MP}/c_{DBSA} = 87:13. The two modes at lower frequencies are caused by the collective motion of nanoplatelets. For higher nanoplatelet concentrations, an additional mode arises, which is attributed to the nematic phase. is discernable.

Conclusion and outlook

The dynamic measurements on BaHF nanoplatelet suspensions with different nanoplatelet and DBSA surfactant concentrations show distinct differences. For low c_{MP} and an optimum ratio c_{MP}/c_{DBSA} = 87:13, a single relaxation mode has been observed which is attributed to the relaxation of individual nanoplatelets. In all other cases, several relaxation modes were observed in ACS as well as in torsional balance measurements. At high c_{MP}, an additional mode was observed, which can be related to the nematic phase.
Our studies demonstrate the importance of optimally adjusting the ratio between magnetic and electrostatic interactions.

Acknowledgment

The research was funded by DFG via projects LU 800/7-1 and NA 1668/1-1.

References

[1] A. Mertelj et al., „Ferromagnetism in suspensions of magnetic platelets in liquid crystal", Nature 504, 237 (2014).
[2] N. Sebastián et al., „Director reorientation dynamics of ferromagnetic nematic liquid crystals", Soft Matter 14, 7180 (2018).
[3] M. Shuai et al., „Spontaneous liquid crystal and ferromagnetic ordering of colloidal magnetic nanoplates", Nature Commun. 7, 10394 (2016).
[4] J. Dieckhoff et al., „Fluxgate based detection of magnetic nanoparticle dynamics in rotating magnetic fields", Appl. Phys. Lett. 99, 112501 (2011).
[5] M. Küster et al., „Magnetic dynamics in suspensions of ferrimagnetic platelets", J. Mol. Liq. 360, 119484 (2022).
[6] T. Yoshida and K. Enpuku, „Simulation and quantitative clarification of ac susceptibility of magnetic fluid in nonlinear Brownian relaxation region", Jpn. J. Appl. Phys. 48, 127002 (2009).
[7] I. Torres-Diaz and C. Rinaldi, „Ferrofluid flow in a spherical cavity under an imposed uniform rotating magnetic field: Spherical spin-up flow", Phys. Fluids 24, 082002 (2012).

On a field-controlled mass transport in concentrated ferrofluids

A.A. Kuznetsov[1], V.S. Zverev[2], S.S. Kantorovich[1]

[1] *University of Vienna, Faculty of Physics, Kollingasse 14-16, 1090 Vienna, Austria*
[2] *Ural Federal University, 51 Lenin Avenue, 620000 Ekaterinburg, Russia*

Magnetophoresis, that is, the motion of magnetic objects under the action of a nonuniform magnetic field, is the physical basis for many applications of magnetic nanoparticles (MNPs) in biotechnology and medicine. Examples of such applications are magnetic cell separation and targeted drug delivery. It is known that the sensitivity of MNPs to the applied gradient field is among main factors determining their suitability for biomedical purposes [1]. In this contribution, we use methods of nonequilibrium statistical mechanics as well as Langevin dynamics simulations to study how the magnetophoretic movement of MNPs in a nonmagnetic viscous medium is affected by various interactions between these MNPs. Specifically, we investigate a concentration redistribution of MNPs in the vicinity of a current-carrying cylindrical conductor. A gradient azimuthal field of the current causes the magnetophoretic drift of MNPs towards the conductor (see Figure 1). This drift is hindered by the Brownian diffusion. Over time, a stable nonuniform concentration profile of MNPs is achieved as a results of competition between magnetophoresis and diffusion. We obtain several sets of these profiles from Langevin dynamics for different values of MNPs dipolar coupling constant and their average concentration. We also estimate the characteristic relaxation times of the drift-diffusion process. Simulation results are used as a verification tool for the mass transport equation first derived in Ref. [2]. We additionally discuss the possibility of phase separation and convective processes in the simulated system.

References

[1] M. Zborowski, J.J. Chalmers, Magnetic Cell Separation, Elsevier (2007)
[2] A.F. Pshenichnikov, E.A. Elfimova, A.O. Ivanov. "Magnetophoresis, sedimentation, and diffusion of particles in concentrated magnetic fluids." JCP 134, 18, 184508 (2011).

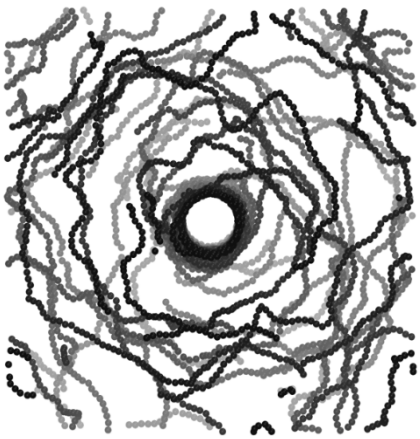

Fig. 1: Simulation snapshot of of the MNP distribution in the vicinity of a current-carrying cylindrical conductor placed in the middle of the simulation box (top view)

Towards FeRh-nanoparticle inks for printable magnetocaloric media

J. Landers[1], S. Salamon[1], R. Nadarajah[2], S. Tahir[2], B. Eggert[1], B. Gökce[2], H. Wende[1]

[1] *Faculty of Physics and Center for Nanointegration Duisburg-Essen (CENIDE), University of Duisburg-Essen*
[2] *Chair of Materials Science and Additive Manufacturing, University of Wuppertal*

FeRh is a well-known prototype material for magnetic refrigeration due to its giant magnetocaloric effect connected to the first-order phase transition close to room temperature. While in bulk dimensions alternative, more abundant materials as compared to rhodium are sought, cooling of e.g. microelectronic devices via printed 2d-structures of magnetocaloric FeRh would be favorable due to the versatility of attainable shapes and the limited amount of necessary FeRh material.
Here, FeRh nanoparticles were prepared via laser ablation in liquids (LAL) under different atmospheres from a $Fe_{50}Rh_{50}$ bulk target as shown in figure 1. Oxide fraction and phase composition were analyzed via XRD and Mössbauer spectroscopy, showing ca. 20% of Fe^{3+}-oxide material in the as-prepared nanoparticles, with the remaining FeRh consisting primarily of the paramagnetic A1-phase and only ca. 3% of magnetically ordered B2-phase due to quenching of the A1 high-temperature phase during the laser heating process. The oxide fraction could be minimized via preparation of the nanoparticles e.g. under argon atmosphere.

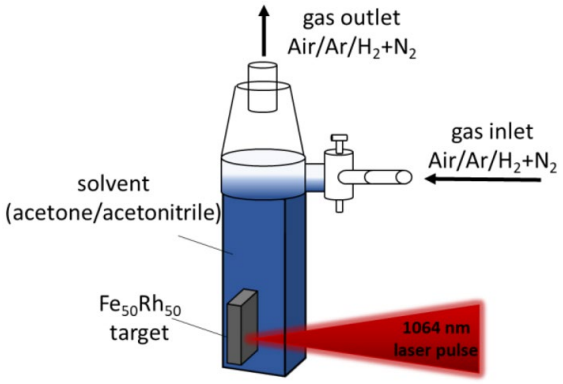

Fig. 1: FeRh nanoparticle preparation via laser ablation in liquid (LAL). [1]

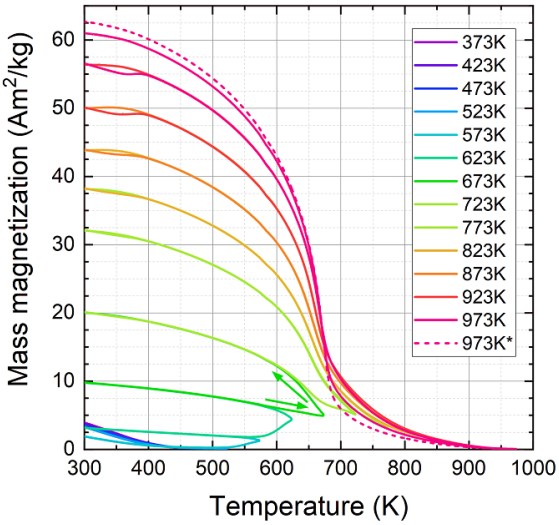

Fig. 2: Conversion of FeRh nanoparticles from the paramagnetic A1- to the magnetically ordered B2-phase by cyclic heating up to 973K recorded at 0.1T. [2]

An increase of the B2-phase fraction in the FeRh nanoparticle powders to >90% could be demonstrated via XRD and magnetometry by conventional (vacuum) heating up to ca. 1000K, starting at ca. 500K, potentially also including a reduction of the oxide fraction. This is reflected by a considerable increase in magnetization and the manifestation of a beginning thermal hysteresis corresponding to the FeRh antiferro- to ferromagnetic (AFM-FM) transition at ca. 370K (see figure 2). However, only a moderate field-induced increase in magnetization was observable for the conventionally heated nanoparticle powders.
To facilitate printable structures directly from the FeRh nanoparticles in solution, the ink was laser-sintered after deposition on a glass substrate. Here, the laser-sintering process combines the recovery of the magnetocaloric B2-phase with the "printing" process of the desired 2D structures.
After testing different laser fluences, an optimum value of ca. 300-400 J/cm^2 was

determined, with lower values leading to only partial A1- to B2 conversion, while high laser fluences result in beginning evaporation of substrate material. For this setting, a composition of ca. 70% B2- and 30% A1-FeRh was found. Ca. 50% of the B2 fraction seem to remain pinned in the ferromagnetic high-temperature state, not participating in the transition. Still, magnetometry displays a pronounced field-induced increase in magnetization at 300-400K due to the field-driven transition from the AFM- to FM-state, indicating the recovery of magnetocaloric properties in the printed structures after laser-sintering.

This is a very promising first result for printable magnetocaloric structures from LAL-made inks. Still, further experiments will have to show the exact magnetocaloric efficiency of the attained structures and to which extent a further increase in B2-fraction, nanoparticle magnetic order and magnetocaloric effect can be obtained via optimization of nanoparticle processing and laser-sintering parameters.

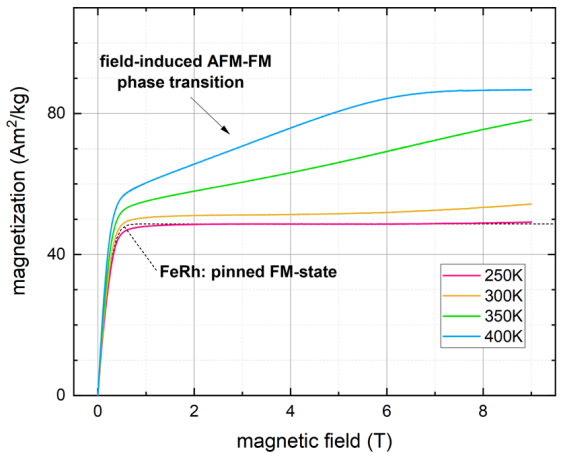

Fig. 3: Laser annealed 2D structures exhibit the AFM-FM transition responsible for FeRh magnetocaloric properties, as visible here by the field-induced increase in magnetization. [3]

Acknowledgments

We gratefully acknowledge funding by the DFG through CRC/TRR 270, projects B5 and B8, and through projects GO2566/2-1 and GO2566/10-1.

References

[1] R. Nadarajah et al. „Controlling the oxidation of magnetic and electrically conductive solid-solution iron-rhodium nanoparticles synthesized by Laser Ablation in Liquids", *Nanomaterials* **10**, 2362 (2020)

[2] R. Nadarajah et al. "Towards laser printing of magnetocaloric structures by inducing magnetic phase transition in iron-rhodium nanoparticles", *Sci. Rep.* **11**, 13719 (2021)

[3] S. Tahir et al., "Laser-assisted direct-writing of magnetocaloric structures using FeRh nanoparticle-based ink", *in preparation*

Peptide Functionalized SPIONs for the Acceleration of Sepsis-Diagnosis

S. Lyer[1, 2], B. Friedrich[1], C. Janko[1,2], H. Unterweger[1,2], S. Cunningham[3], S. Dutz[4], H. Hackstein[5], R. Strauß[6], C. Bogdan[7], C Alexiou[1] and R Tietze[1]

[1] *Department of Otorhinolaryngology, Head and Neck Surgery, Section for Experimental Oncology and Nanomedicine (SEON), Else Kröner-Fresenius-Stiftung-Professorship, University Hospital Erlangen, Germany.*
[2] *Professorship for AI-guided Nanomaterials, Department of Otorhinolaryngology, Head and Neck Surgery, University Hospital Erlangen, Germany.*
[3] *Department of Transfusion Medicine and Hemostaseology, Universitätsklinikum Erlangen, Germany.*
[4] *Institute of Biomedical Engineering and Informatics (BMTI), Technische Universität Ilmenau,Germany.*
[5] *Department of Transfusion Medicine and Hemostaseology, Universitätsklinikum Erlangen,Germany.*
[6] *Department of Medicine 1, Universitätsklinikum Erlangen, Germany.*
[7] *Mikrobiologisches Institut – Klinische Mikrobiologie, Immunologie und Hygiene, Universitätsklinikum Erlangen, Friedrich-Alexander-Universität (FAU) Erlangen-Nürnberg, Germany.*

Introduction

Sepsis is an exaggerated immune response to severe infections of the bloodstream [1] affecting an estimated number of annually more than 30 million cases worldwide [2] requiring rapid and directed therapy. Due to the large number of patients, the large proportion of undiagnosed or untimely diagnosis of the causing microorganisms and hence the high mortality rate, improvements and especially acceleration of diagnostics and directed therapy are urgently needed. To tackle this urgent need, SEON has created a strategy based on the use superparamagnetic nanoparticles (SPIONS) functionalized with a binding peptide originating from a large human protein (GP340), which is member of the family of scavenger receptor cysteine rich (SRCR) proteins and part of the innate immune system. This peptide has a highly conserved binding motive revealing a very broad binding range of microorganisms, but is not interfering with any parameters of human blood [3, 4]. With these SPIONs, we were able to develop a reliable biomimetic strategy for a targeted yet broad magnetic separation of bacterial pathogens in bloodstream infections for acceleration of pathogen diagnostics [5, 6].

Results

Synthesis of SPION-APTES-Pep

For directional binding of peptides or proteins, we developed SPIONs consisting of Fe_3O_4 clusters coated with a 3-(Aminopropyl)triethoxysilane (APTES) surface. The coatings formed after polycondensation are characterized by high stability and by the exposure of primary amino groups, subsequently functionalized with succinimidyl bromoacetate (SBA). Finally, approximately 0.094 µmol per mg Fe of the scavenging peptides were covalently bound to this surface via the sulfhydryl group of their C-terminal cysteines (Fig. 1).

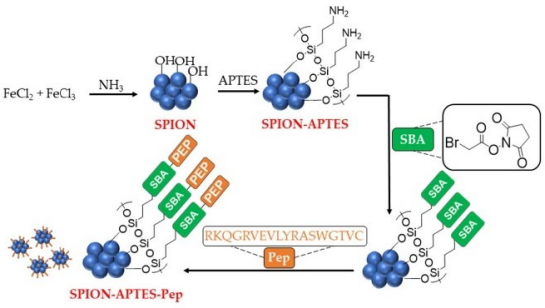

Fig. 1 Route of synthesis of SPION-APTES-Pep.

Characterization of SPIN-APTES-Pep

During the process of functionalization, the ζ potential of SPION-APTES decreased from +49.2 mV to +29.0 mV for SPION-APTES-Pep, and slight precipitation occurred after 3 h. X-ray diffraction analysis (XRD) patterns confirmed the presence of magnetite/maghemite-related characteristic peaks. VSM-measurements showed a saturation magnetization of SPION-APTES of 61.4 Am^2/kg decreasing to 45 Am^2/kg after functionalization with the peptide. Nevertheless, SPION-APTES-Pep could be separated from platelet-poor plasma (PPP) after only 3 min of magnetic separation.
Corresponding bio- and hemocompatibility studies showed that the particles were

fully cyto- and hemo-compatible and did not affect blood parameters such as cytokine release or coagulation.

Pathogen Separation

In blood spiked with bacterial toxins or pathogenic bacteria, we subsequently demonstrated that SPION-APTES-Pep, can magnetically separate a variety of different microbial surface molecules (lipopolysaccharides (LPS) and lipotaichoic acids LTA)) and even intact microorganisms (*E. coli*, *S. aureus*, *P. aeruginosa and S. marcescens*) with high efficiency, especially at low and thus clinically relevant concentrations (Fig. 2). The time of blood sample incubation with the particles and separation was below 10 minutes. The experiments further revealed that the targeting also allowed isolation of intact bacteria and their subsequent enrichment and recultivation without the need for conventional blood culture procedures lasting usually 8 h – 72 h.
We also showed that the magnetic separation of the pathogens from the blood led to a strong decrease in the release of important cytokines (TNF, IL-6, IL-1β, Il-10, and IFN-γ) caused by the bacteria. This could have a direct therapeutic impact as an escalating immune system response complicates the course of severe bloodstream infections and sepsis.

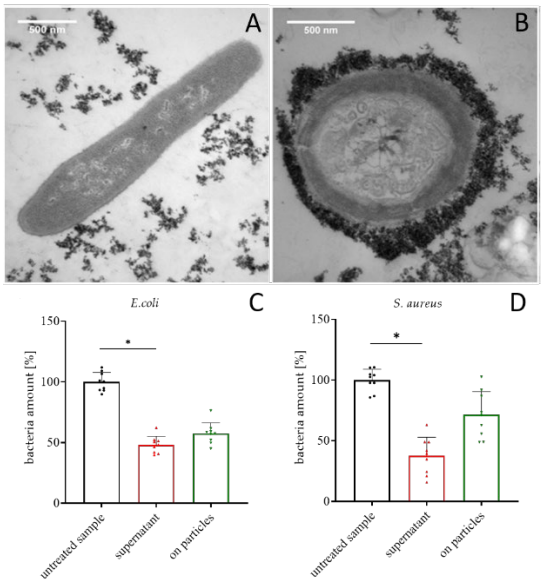

Fig. 2 Separation of bacteria from water-based media and blood. The number of bacteria was set to ~10^3 CFU per mL. Separation was carried out in 1 ml of citrate stabilized blood. a) and b) TEM image of separated E. coli and S. aureus bound to SPION-APTES-Pep after separation. C) and D) Separation and replating efficiency of E. coli and S. aureus after incubation with SPION-APTES-Pep, magnetic separation and 2 washing steps (< 15 min).

Conclusion

In this pilot study we show a fast, reliable, effective and sensitive method for magnetically extracting pathogens from human blood samples using SPION-APTES-Pep. Further development of this technique could help to solve one of the most important problems in sepsis diagnosis – time to pathogen identification.

Acknowledgments

This study was supported by the Doktor Robert Pfleger-Stiftung, Bamberg.

References

[1] Huerta LE, Rice TW. *Pathologic Difference between Sepsis and Bloodstream Infections*. The Journal of Applied Laboratory Medicine 2019, 3 (4), 654-663.

[2] Rudd KE, Johnson SC, Agesa, KM, Shackelford KA, Tsoi, D, Kievlan, D R, Colombara, DV, Ikuta, KS, Kissoon, N, Finfer, S, Fleischmann-Struzek, C, Machado, FR, Reinhart, KK, Rowan, K, Seymour, CW, Watson, RS, West, TE, Marinho, F, Hay, SI, Lozano, R, Lopez, A D, Angus, D C, Murray, C J L, Naghavi, M. *Global, regional, and national sepsis incidence and mortality, 1990–2017: analysis for the Global Burden of Disease Study*. The Lancet 2020, 395 (10219), 200-211.

[3] Bikker FJ, Ligtenberg AJ, Nazmi K, Veerman EC, van't Hof W, Bolscher JG, Poustka A, Nieuw Amerongen AV, Mollenhauer J. *Identification of the bacteria-binding peptide domain on salivary agglutinin (gp-340/DMBT1), a member of the scavenger receptor cysteine-rich superfamily*. J Biol Chem 2002, 277 (35), 32109-15.

[4] End C, Bikker F, Renner M, Bergmann G, Lyer S, Blaich S, Hudler M, Helmke B, Gassler N, Autschbach F, Ligtenberg AJM, Benner A, Holmskov U, Schirmacher P, Amerongen AVN, Rosenstiel P, Sina C, Franke A, Hafner M, Kioschis P, Schreiber S, Poustka A, Mollenhauer J. *DMBT1 functions as pattern recognition molecule for poly-sulfated and poly-phosphorylated ligands*. Eur J Immunol 2009, 39 (3), 833-842.

[5] Karawacka W, Janko C, Unterweger H, Muhlberger M, Lyer S, Taccardi N, Mokhir A, Jira W, Peukert W, Boccaccini A R, Kolot M, Strauss R, Bogdan C, Alexiou C, Tietze R. *SPIONs functionalized with small peptides for binding of lipopolysaccharide, a pathophysiologically relevant microbial product*. Colloids Surf B Biointerfaces 2019, 174, 95-102.

[6] Friedrich B, Lyer S, Janko C, Unterweger H, Brox R, Cunningham S, Dutz S, Taccardi N, Bikker FJ, Hurle K, Sebald H, Lenz M, Spiecker E, Fester L, Hackstein H, Strauß R, Boccacccini AR, Bogdan C, Alexiou C and Tietze R. Scavenging of bacteria or bacterial products by magnetic particles functionalized with a broad-spectrum pathogen recognition receptor-motif offers diagnostic and therapeutic applications. Acta Biomater 2022 Mar; 15;141:418-428. Epub 2022 Jan 7.

Targeted cell seeding of human vocal fold fibroblasts via superparamagnetic iron oxide nanoparticles

Felix Pfister[1], Mona Kappes[1], Bernhard Friedrich[1], Christian Huber[1,2], Ralf Phillipp Friedrich[1], René Stein[1], Christian Braun[3], Stefan Lyer[1], Julia Band[1], Eveline Schreiber[1], Christoph Alexiou[1], Christina Janko[1]

[1] Department of Otorhinolaryngology, Head and Neck Surgery, Section of Experimental Oncology and Nanomedicine (SEON), Else Kröner-Fresenius-Stiftung Professorship, Universitätsklinikum Erlangen, 91054 Erlangen, Germany. E-mail: felix.pfister@uk-erlangen.de
[2] Institute of Microwave and Photonics, Friedrich-Alexander-Universität Erlangen-Nürnberg, 91058 Erlangen, Germany.
[3] Institute of Legal Medicine, Ludwig-Maximilians-Universität München, 80336 München, Germany.

Introduction

Injury of the vocal fold causes major impairment on the patient's quality of life. To this day, no sufficient treatment for vocal fold tissue regeneration exists. Tissue engineering represents an important part of regenerative medicine focused on the restoration of tissues and even organs [1]. However, the vocal fold is a complex structure consisting of multiple specialized cell types. The recreation of these layers is a difficult and a lengthy task.
Cells loaded with superparamagnetic iron oxide nanoparticles (SPIONs) allow their controlled movement by an external magnetic field. These SPIONs have already been used to establish 3D constructs of human vocal fold fibroblasts (VFF) [2].
In this study, we have investigated the ability of differently-coated SPIONs on the formation of spheroids and magnetic patterning of primary human VFFs compared to the commercially available NanoShuttle-PL.

Results

VVF cells were isolated directly from human cadavers as already described and loaded *ex vivo* for further analysis [3]. Polyacrylic acid-co-maleic acid (PAM)- or Citrate-coated SPIONs were synthesized in-house as previously depicted [4, 5].

Acceleration of Spheroid formation

For the formation of VFF spheroids, the cells were loaded with the respective nanoparticles. Then, the cells were seeded in cell repellent U-plates placed above a micromagnet array. After 3 h, the 2D area of the spheroids was investigated by microscopy and the area was measured. The addition of SPIONs and an external magnetic field resulted in an accelerated spheroid formation, with a reduction of almost 50% in the mean spheroid area of citrate-coated SPION-loaded VFF compared to only 9% in VFF spheroids without SPIONs.

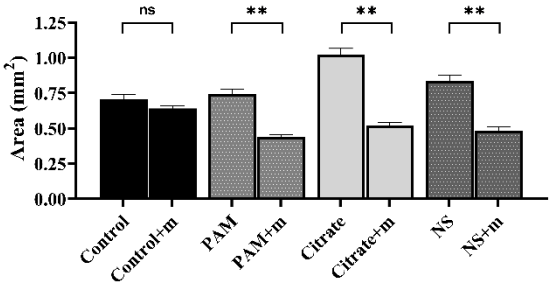

Fig. 1 *Spheroid formation is accelerated by SPION-loading. Loaded VFF cells were seeded in a cell repellent U-plate without or above a micromagnet array (+m). The spheroid area was measured 3 h after seeding.*

Magnetic Patterning

The generation of different cellular structures via SPIONs requires the magnetic guidance and thus the enrichment of cells in specific regions. Therefore, a ring magnet was placed under SPION-loaded VFF cells for 24 h. To evaluate the ring formation, the magnetic field was simulated and superimposed over the microscopy images of the cells. VFF loaded with PAM-coated SPIONs formed the most distinct shape compared

to citrate-coated SPIONs or NanoShuttle-PL.

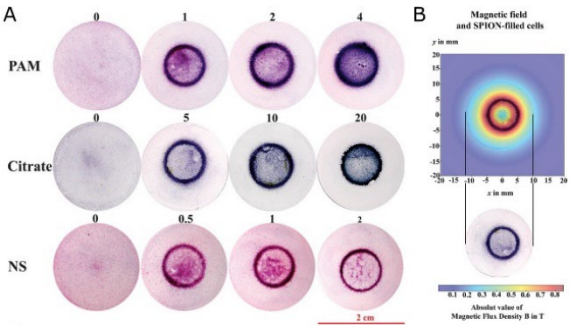

Fig. 2 *Magnetic patterning of SPION-loaded hVFF. A) Macroscopic ring patterning of Hematoxylin–Eosin and Prussian Blue-stained fibroblasts. B) Overlay of the macroscopic patterning with a simulated magnetic flux density in the xy-plane.*

Magnetic Spheroid Micropatterning

Tissue is composed of different cells at distinct locations, therefore we investigated the ability of SPIONs to create spheroids with polar cell populations. VFF cells were loaded with the respective nanoparticles and seeded in a cell-repellent plate with a magnetic spheroid drive placed below. Unloaded VFF cells were added to the wells as well. After 24 h, the spheroids were investigated by fluorescence microscopy. A janus-like structure could be detected for PAM-coated, citrate-coated SPIONs, or NanoShuttle-PL. This indicates the possibility of creating layered cell structures via an external magnetic field.

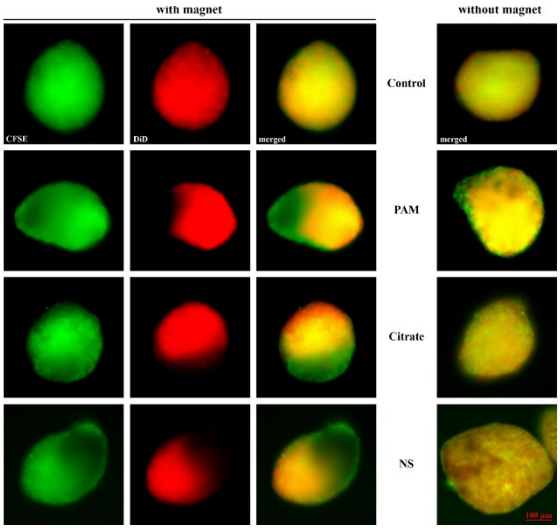

Fig. 3 *SPION-induced micropatterning in VFF spheroids. CFSE-stained VFF cells were loaded with the respective nanoparticles (green) and co-incubated with DiD-stained unloaded VFF (red). The cells were then cultivated on a magnetic spheroid drive for 24 h and subsequently imaged by fluorescence microscopy.*

Conclusion

We have shown an easy, fast and reproducible method for the magnetic patterning of primary human VFF mediated by the use of differently coated SPIONs compared to the commercially available NanoShuttle-PL. Further improvements could reduce the complexity and time needed for the production of multicellular structures in tissue engineering.

Acknowledgments

This study was supported by the Else Kröner-Fresenius-Stiftung (No. 2018_A88), Bad Homburg v.d.H, Germany.

References

1. Berthiaume, F., T.J. Maguire, and M.L. Yarmush, *Tissue engineering and regenerative medicine: history, progress, and challenges.* Annu Rev Chem Biomol Eng, 2011. **2**: p. 403-30.
2. Pottler, M., et al., *Magnetic Tissue Engineering of the Vocal Fold Using Superparamagnetic Iron Oxide Nanoparticles.* Tissue Eng Part A, 2019. **25**(21-22): p. 1470-1477.
3. Kappes, M., et al., *Superparamagnetic Iron Oxide Nanoparticles for Targeted Cell Seeding: Magnetic Patterning and Magnetic 3D Cell Culture.* Adv. Funct. Materials, 2022.
4. Blumler, P., et al., *Contactless Nanoparticle-Based Guiding of Cells by Controllable Magnetic Fields.* Nanotechnol Sci Appl, 2021. **14**: p. 91-100.
5. Mühlberger, M., et al., *Functionalization Of T Lymphocytes With Citrate-Coated Superparamagnetic Iron Oxide Nanoparticles For Magnetically Controlled Immune Therapy.* Int J Nanomedicine, 2019. **14**: p. 8421-8432.

Field-Controlled Bending of a Multipole Magneto-active Elastomer for Vibration-Driven Locomotion

M. Reiche[1], T. I. Becker[1], G. V. Stepanov[2], F. Becker[3], K. Zimmermann[1]

[1] *Technical Mechanics Group, Faculty of Mechanical Engineering, Technische Universität Ilmenau, 98684 Ilmenau, Germany*
[2] *State Scientific Research Institute of Chemistry and Technology of Organoelement Compounds, 111123 Moscow, Russia*
[3] *Technical Mechanics Group, Faculty of Automotive Engineering, University of Applied Sciences Zwickau, 08056 Zwickau, Germany*

Magnetoactive elastomers (MAEs) combine elastic and magnetic properties that can be to a large extent modified in response to a magnetic field. When such an elastomer contains micro-sized magnetically hard particles of highly coercive ferromagnetic material, it becomes an elastic magnet once magnetized in a strong impulse magnetic field. The magnetically soft particles in the elastomer are used to obtain additional advantageous features such as enhanced magnetization and magnetic susceptibility.

Motion systems based on MAEs have been gaining increasing research interest in the field of soft robotics and related technologies in recent years. Compared to traditional robots that use several rigid links and joints to attain a needed configuration, mobile robots made of deformable magnetic bodies can be realized with a minimal number of actuators [1, 2]. In this work, we present a multipole magnetized MAE element incorporating both magnetically hard and soft particles to create a vibration-driven locomotion system [3]. The MAE element is fabricated in a way that it has three poles overall with the same poles at both ends (Fig. 1). The bending deformation of the multipole MAE element in vertical plane is caused by an external or integrated magnetic field sources. Either an external large-sized Helmholtz coil or a small coil integrated into the system's frame is used. Since the MAE element is made and magnetized with a reflection symmetry, it bends symmetrically about the vertical axis passing through its center, thereby shifting positions of the both ends. To create directional locomotion of the element resulting from this bending, some asymmetry to the system is introduced. The change of contact conditions to the ground is realized by silicone "bristles" protruding at an oblique angle from the underside of the MAE element. The provided asymmetric friction ensures a preferred directed locomotion in each cycle of oscillation controlled by an alternating magnetic field.

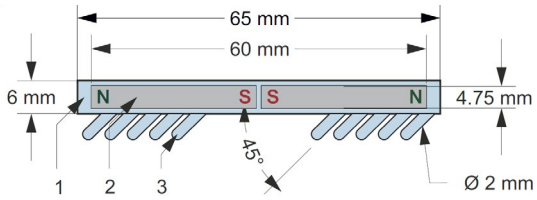

Fig. 1: MAE functional element: 1 - silicone casing, 2 - multipole magnetized MAE beam, 3 - rows of silicone bristles.

The quasi-static bending of the multipole magnetized MAE functional element is investigated experimentally in a uniform magnetic field directed either upward or downward. The MAE element standing on its bristles is placed on a non-magnetic horizontal base in the middle of a Helmholtz coil with a vertical axis. The deflected shape is measured using a laser triangulation sensor, which is attached above the MAE element to a horizontal linear axis and measures a vertical distance to its upper side. When the field is applied upward, the element bends to a U-shape, which becomes more pronounced with increasing field magnitude. The downward direction of the applied field causes an inverted U-shape of bending.

The locomotion system consists of the multipole magnetized MAE functional element with an additively manufactured top part, on which an integrated elec-

tromagnetic coil is fixed in the middle. The coil is supplied by a current source and controlled by an H-bridge that provides the required modulation of a voltage applied. The current is a square wave alternating positive and negative with an amplitude of ±168 mA. Excitation frequencies are applied in the wide range of f = 5-130 Hz. Figure 2 compares the distances traveled by the system in equal time intervals for four different excitation frequencies. Among the chosen frequency values, the motion at f = 75 Hz is the fastest, since this frequency belongs to the resonance range of the system. The maximum advancing speed of 70.4 mm/s is achieved by this excitation.

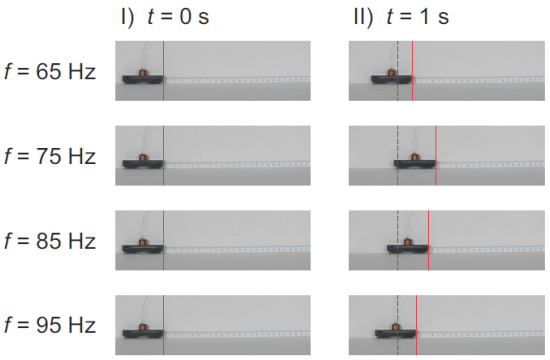

Fig. 2: Comparison of distances covered by the locomotion system at different excitation frequencies of the integrated coil.

The advancing speed of the locomotion system for the whole range of excitation frequencies is shown in Fig. 3. For frequencies below the resonant range, the speed first grows slowly with increasing frequency, and then it rises steeply to the resonance peak. When the frequency is above the resonant range, there is an almost continuous decrease of the advancing velocity over the frequency. On the whole, the key advantages of the locomotion system are the high speed of movement and at the same time a rather simple and easy-to-implement method of magnetic actuation.

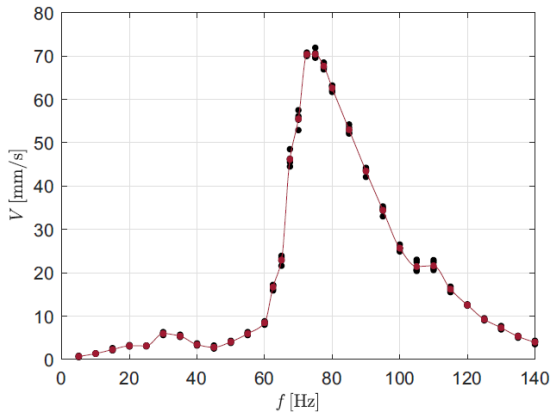

Fig. 3: Advancing speed of the locomotion system dependent on the excitation frequency of alternating magnetic field of the integrated coil.

Acknowledgments

The work is funded by the research association PAK907 between the Deutsche Forschungsgemeinschaft (DFG) and the Russian Foundation for Basic Research (RFBR) under the projects BE-6553/2-1 and 19-53-12039.

References

[1] Zimmermann K., Böhm V., Zeidis I. Vibration-driven mobile robots based on magnetosensitive elastomers. In: 2011 IEEE/ASME Int. Conf. on Adv. Intelligent Mechatronics (AIM2011). Budapest, Hungary (2011) p. 730-735.

[2] Zimmermann K., Naletova V.A., Zeidis I., Turkov V.A., et al. A deformable magnetizable worm in a magnetic field - A prototype of a mobile crawling robot. J. Magn. Magn. Mater. 311(1) (2007) p. 450-453.

[3] Reiche M., Becker T.I., Stepanov G.V., Zimmermann K. A Multipole Magnetoactive Elastomer for Vibration-Driven Locomotion. Submitted to Soft Robotics (2022).

Hydrothermal Synthesis of Barium Hexaferrite Nanoparticles

B. Rhein, S. Ranoo, A. M. Schmidt

Department Chemistry, Institute for Physical Chemistry, University of Cologne Greinstraße 4 - 6, 50939 Cologne

Abstract

Barium hexaferrite ($BaFe_{12}O_{19}$, BaM) is a ferrimagnetic metal oxide of the hexagonal ferrite type. It is of exceptional volume magnetization, high magneto-crystalline anisotropy, and good chemical stability, making it an attractive material for various applications like magnetic recording and storage, permanent magnets, and microwave devices [1] [2].

Barium hexaferrite can be synthesized via techniques such as co-precipitation, salt melt method, microemulsion method, glass crystallization method, sol-gel, combustion technique, and hydrothermal methods [1]. Under appropriate synthetic conditions, its growth can be predominantly directed to the ab plane, leading to BaM nanoparticles with a platelet shape. In these platelets, the preferred direction of magnetization is perpendicular to the particle surface. These properties qualify such BaM nanoplatelets as an attractive candidate for the fabrication of anisotropic nanocomposite and smart magnetic materials.

The barium hexaferrite particles presented here are synthesized by a hydrothermal route [3] in aqueous conditions. The influence of synthesis temperature, precursor concentration, and reaction time on the size distribution, morphology, and magnetic properties are investigated.

The particles are characterized by transmission electron microscopy (TEM) and vibrating sample magnetometry (VSM). It is found that the particles possess a nanoplatelet shape (s. Fig. 1). The size distribution and the mean size change with the reaction temperature. While at low reaction temperature, mainly small nanoplatelets of 30 nm are observed, with increasing temperature triangular or hexagonal platelets of about 300 nm - 320 nm evolve. In quasi-static magnetization experiments, nanoplatelets showed hysteretic behavior as a powder, while their aqueous dispersion was of pseudo- superparamagnetic response. It is observed that the squareness (M_R/M_S) value of the nanoplatelet powders increases with increasing synthesis temperature.

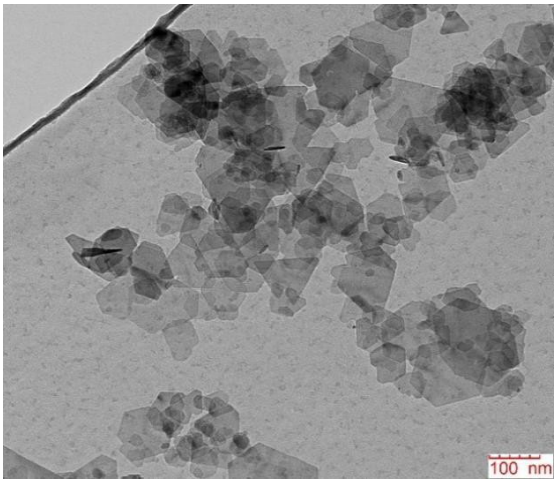

Figure 1 TEM image of the barium hexaferrite nanoplatelets

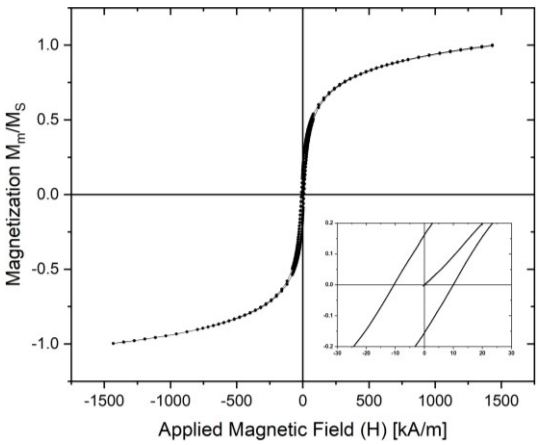

Figure 2 Magnetic hysteresis loop of barium hexaferrite measured at room temperature

In ongoing works, the reaction parameters are optimized in order to allow for tuning the magneto-crystalline properties of the

barium hexaferrite nanoplatelets for various applications.

References

[1] R. C. Pullar, "Hexagonal ferrites: A review of the synthesis, properties and applications of hexaferrite ceramics," *Progress in Materials Science,* pp. 1191-1334, 2012.

[2] D. Makovec, B. Belec, T. Goršak, D. Lisjak, M. Komelj, G. Dražić and S. Gyergyek, "Discrete evolution of the crystal structure during the growth of Ba-hexaferrite nanoplatelets," *Nanoscale,* pp. 14480-14491, 2018.

[3] M. Drofenik, i. Ban, G. Ferk, D. Makovec, A. Znidarsic, Z. Jaglicic and D. Lisjak, "The Concept of a Low-Temperature Synthesis for Superparamagnetic BaFe12O19 Particles," *Journal of the American Ceramic Society,* vol. 93, no. 6, pp. 1602-1602, 2010.

Ferrite-based Magnetic Nanoparticles in a Smart Polymer Matrix

M. Weißpflog and B. Hankiewicz

Institute of Physical Chemistry, University of Hamburg, Grindelallee 117, 20146 Hamburg, Germany
maria.weisspflog@chemie.uni-hamburg.de, birgit.hankiewicz@chemie.uni-hamburg.de

For hyperthermia applications, reproducible synthesis routes of magnetic nanoparticles (MNP) with control and adjustment of the structure, size, shape and magnetic properties are the key aspects. To minimize the adverse side effects on healthy cells, a large amount of heat generated by a small quantity of nanoparticles must be delivered to the tumor cells only. Therefore, particles with large values of saturation magnetization and a high resolution for magnetic imaging are required leading to a strong and efficient response to the external magnetic field. Moreover, by increasing the saturation magnetization values, the control over the movements of the MNP can be optimized by the external magnetic field after injection into the bloodstream so the required therapeutic concentration of MNP can be reduced accordingly. Among the ferrites, magnetite (Fe_3O_4) has the largest magnetic moment, but it grows into an isotropic form for thermodynamic reasons and has a correspondingly small magnetic anisotropy constant. In previously published papers on magnetite, it has been shown that anisotropic particles have higher magnetic anisotropy constants than spherical particles and, thus, higher coercive field strengths to avoid rapid demagnetization.[1–3] It is also known that anisotropic iron oxides have a higher saturation magnetization than spherical ones.[4] Furthermore, cobalt ferrite ($CoFe_2O_4$) has turned out to be an interesting material as spherical cobalt ferrite shows a higher magnetocrystalline anisotropy than iron oxide.[5,6] As the reduction of the Co^{2+} ion concentration in cobalt ferrite particles leads to an increase in average crystallite size, coercivity, and saturation magnetization,[2,5,7] our work is focused on the synthesis of non-stoichiometric cobalt ferrite nanoparticles. In a two-step reaction, akageneite nanorods (an antiferromagnetic iron oxide hydroxide) were prepared first followed by an aqueous hydrothermal reaction without toxic surfactants or solvents and variation of the metal salt concentration and composition of $Co^{2+}/Fe^{3+}/Fe^{2+}$.
Examination of the magnetic characteristics of the nanoparticles and hyperthermia measurements will be systematically conducted to consolidate the heating efficiency of the as-synthesized MNP. These particles should already be dominated by the Brownian relaxation mechanism in the high single-digit nanometer range from about 7 nm compared to magnetite nanoparticles, which are dominated by the Néelian relaxation mechanism up to a critical particle diameter above 14 nm.[8] Additionally, the magnetic properties can be optimized through the occurrence of the exchange bias effect with the help of a core-shell system, a magnetic coating, or an ion exchange on the surface of antiferromagnetic nanoparticles.[9,10]

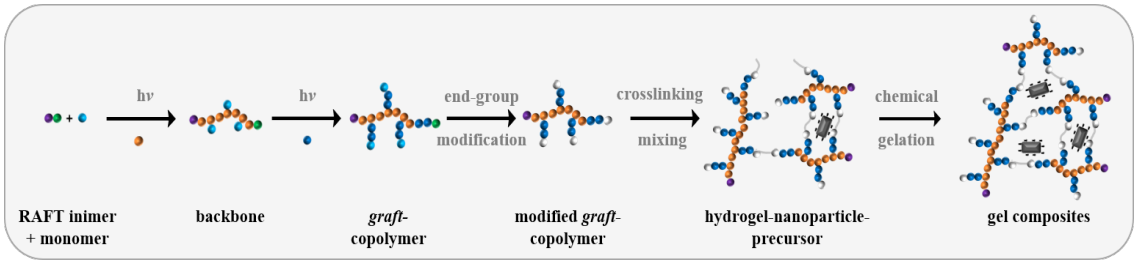

Figure 1. *Schematic synthesis of a hydrogel-nanoparticle composite combined by a thermoresponsive graft-copolymer prepared by RAFT polymerization and embedded cobalt ferrite particles. Selective initiation of the backbones and side chains are performed by two kinds of visible light irradiation.*

An extensive field in material science is developed by embedding these "hard" magnetic nanostructures within an organic "soft" matter. In our working group, we will focus on the combination of magnetic cobalt ferrite and magnetite with a crosslinked gel matrix consisting of a double thermoresponsive *graft*-copolymer. For the synthesis of the polymers, initiator-free photoiniferter reversible addition-fragmentation chain transfer (RAFT) polymerization will be used due to selective initiation of the backbones and side chains from acrylic and methacrylic monomers.[11–13] The number and length of the side chains will significantly influence the mesh size of the gel and, thus, the incorporation of the MNPs. In addition, subsequent conversion of the trithiocarbonate pendant groups to thiol reactive functionalities enables further modification and covalently crosslinking to afford a thermoresponsive hydrogel and, exemplarily, application in the field of polymer therapeutics.

References

(1) Geng, S.; Yang, H.; Ren, X.; Liu, Y.; He, S.; Zhou, J.; Su, N.; Li, Y.; Xu, C.; Zhang, X.; Cheng, Z. Anisotropic Magnetite Nanorods for Enhanced Magnetic Hyperthermia. *Chemistry, an Asian journal* **2016**, *11* (21), 2996–3000. DOI: 10.1002/asia.201601042. Published Online: Oct. 6, 2016.

(2) Mitra, A.; Mohapatra, J.; Sharma, H.; Aslam, M. Engineering Magnetic and Tunneling Magnetoresistance Properties of Co x Fe 3−x O 4 Nanorods. *Phys. Status Solidi A* **2017**, *214* (12), 1700505. DOI: 10.1002/pssa.201700505.

(3) Yang, Z.; Yao, K. Effects of several kinds of anisotropy on the coercivity behaviors of iron oxides. *Journal of Applied Physics* **1993**, *73* (10), 6665–6667. DOI: 10.1063/1.352549.

(4) Virden, A.; Wells, S.; O'Grady, K. Physical and magnetic properties of highly anisotropic cobalt ferrite particles. *Journal of Magnetism and Magnetic Materials* **2007**, *316* (2), e768-e771. DOI: 10.1016/j.jmmm.2007.03.100.

(5) Yasemian, A. R.; Almasi Kashi, M.; Ramazani, A. Exploring the effect of Co concentration on magnetic hyperthermia properties of Co x Fe 3−x O 4 nanoparticles. *Mater. Res. Express* **2020**, *7* (1), 16113. DOI: 10.1088/2053-1591/ab6a51.

(6) Fayazzadeh, S.; Khodaei, M.; Arani, M.; Mahdavi, S. R.; Nizamov, T.; Majouga, A. Magnetic Properties and Magnetic Hyperthermia of Cobalt Ferrite Nanoparticles Synthesized by Hydrothermal Method. *J Supercond Nov Magn* **2020**, *33* (7), 2227–2233. DOI: 10.1007/s10948-020-05490-6.

(7) Ayyappan, S.; Philip, J.; Raj, B. Effect of Digestion Time on Size and Magnetic Properties of Spinel CoFe 2 O 4 Nanoparticles. *J. Phys. Chem. C* **2009**, *113* (2), 590–596. DOI: 10.1021/jp8083875.

(8) Odenbach, S. *Colloidal Magnetic Fluids*, Vol. 763; Springer Berlin Heidelberg, 2009. DOI: 10.1007/978-3-540-85387-9.

(9) Lu, A.-H.; Salabas, E. L.; Schüth, F. Magnetic nanoparticles: synthesis, protection, functionalization, and application. *Angewandte Chemie (International ed. in English)* **2007**, *46* (8), 1222–1244. DOI: 10.1002/anie.200602866.

(10) Winkler, E. L.; Lima, E.; Tobia, D.; Saleta, M. E.; Troiani, H. E.; Agostinelli, E.; Fiorani, D.; Zysler, R. D. Origin of magnetic anisotropy in ZnO/CoFe 2 O 4 and CoO/CoFe 2 O 4 core/shell nanoparticle systems. *Appl. Phys. Lett.* **2012**, *101* (25), 252405. DOI: 10.1063/1.4771993.

(11) Shanmugam, S.; Cuthbert, J.; Kowalewski, T.; Boyer, C.; Matyjaszewski, K. Catalyst-Free Selective Photoactivation of RAFT Polymerization: A Facile Route for Preparation of Comblike and Bottlebrush Polymers. *Macromolecules* **2018**, *51* (19), 7776–7784. DOI: 10.1021/acs.macromol.8b01708.

(12) Corrigan, N.; Trujillo, F. J.; Xu, J.; Moad, G.; Hawker, C. J.; Boyer, C. Divergent Synthesis of Graft and Branched Copolymers through Spatially Controlled Photopolymerization in Flow Reactors. *Macromolecules* **2021**, *54* (7), 3430–3446. DOI: 10.1021/acs.macromol.0c02715.

(13) Arrington, K. J.; Matson, J. B. Assembly of a visible light photoreactor: an inexpensive tool for bottlebrush polymer synthesis via photoiniferter polymerization. *Polym. Chem.* **2017**, *8* (48), 7452–7456. DOI: 10.1039/C7PY01741C.

Low-cost standalone magnetic particle spectroscopy device for fast and sensitive immunoassays

Florian Wolgast, Tamara Kahmann, Enja Rösch, Aidin Lak, Meinhard Schilling, Frank Ludwig, Thilo Viereck

Institut für Elektrische Messtechnik und Grundlagen der Elektrotechnik (EMG) and LENA, TU Braunschweig, Braunschweig, Germany

The recent pandemic has shown how important reliable assays are for determining whether someone is infectious. In order to be better prepared for high test demand and possible supply shortages, it is important to have a wide availability of different assays. One promising alternative to the established PCR and antigen quick tests based on lateral flow devices with colloidal gold nanoparticles are immunoassays with magnetic nanoparticle (MNP) markers. Especially, magnetic particle spectroscopy (MPS) promises fast and quantitative point-of-need testing with a compact device. In MPS, the MNP markers are exposed to an alternating magnetic field of sufficiently large amplitude for measuring the dynamic magnetization response which contains the fundamental and several harmonic frequencies. Due to the fast and highly sensitive measurement principal MPS is well suited for magnetic immunoassays.

In this work, we present the development of our "immunoMPS" (Fig. 1) which was especially built for immunoassays with infectious samples. Therefore, the device is at low cost, fully self-contained, mobile and could be used in a S2+ bio-safety lab. The device works with an excitation frequency of 590 Hz optimized for BNF80 nanoparticles from micromod Partikeltechnologie GmbH to capture Brownian relaxation dynamics. It delivers high performance (on par or exceeding our lab equipment) for material costs around 300 Euro. We are currently working towards DNA- and antibody(AB)-based immunoassays for SARS-CoV-2. Preliminary results on both strategies have been published [1, 2]. For the AB-immunoassays several groups have proven the use of MNP for SARS-CoV-2 detection with a limit of detection (LOD) around 10^9-10^{10} virus/mL [1][3]. While the work by Wu et al. [3] focused on the detection of the SARS-CoV2 spike and N-proteins, our previous work used mimic viruses [1] and DNA [2] as biological targets.

Figure 1: Picture of our "immunoMPS" device

Together, the results demonstrate the versatility of magnetic nanoparticle bioassays in combination with the MPS platform. However, for a reliable detection of spread-infectious persons a threshold of around 10^4-10^{10} virus/mL is required. Consequently, the LODs of most current magnetic immunoassays are not good enough to detect low virus loads. In our recent experiments, which were all performed on the new device, we reach a 3σ LOD of 4×10^8 virus/mL (0.06 fmol) (Fig. 2).

Currently, we are working towards lower MNP and especially antigen and DNA

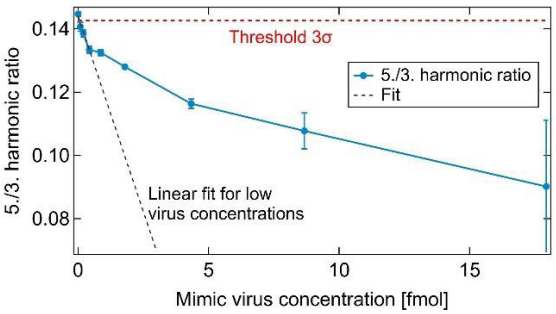

Figure 2: Harmonic ratio 5th/3rd from the MPS measurements of different mimic virus concentrations in an AB-immunoassay with mimic viruses

detection limits with an optimized setup, on improved assay protocols and tailored materials. On the measurement instru-

ment side, we try to achieve an improved detection limit by using a mixing frequency method (MFM). In this approach, the excitation of the magnetic nanoparticles is done with an additionally high-frequency magnetic field with small amplitude compared to conventional MPS. The advantage of this method is that the resulting mixed harmonics are highly specific to the nonlinear magnetization curve of the MNP [4]. On the other hand, for example, the assay protocol is improved by systematically investigating the influence of different incubation methods as well as the amount of antibody per magnetic nanoparticle.

Acknowledgments

DFG: EXC-2123 Quantum Frontiers Germany's Excellence Strategy – 390837967, Research Training Group 1952 Metrology for Complex Nanosystems, ZH 782/1-1.
Niedersächsisches Vorab: Quantum and NanoMetrology (QUANOMET) initiative projects NL-1 (BL) and NP-2 (TV).

References

[1] Zhong et al., "Toward Rapid and Sensitive Detection of SARS-CoV-2 with Functionalized Magnetic Nanoparticles", ACS Sensors 0c02160 (2021), DOI: 10.1021/acssensors.0c02160

[2] Roesch et al., "Point-of-need detection of pathogen-specific nucleic acid targets using magnetic particle spectroscopy", Biosens. Bioelectron. 192, 113536 (2021), DOI: 10.1016/j.bios.2021.113536

[3] Wu et al., "One-Step, Wash-free, Nanoparticle Clustering-Based Magnetic Particle Spectroscopy Bioassay Method for Detection of SARS-CoV-2 Spike and Nucleocapsid Proteins in the Liquid Phase", ACS Appl. Mater. Interfaces 13, 37, 44136 – 44146 (2021), DOI: 10.1021/acsami.1c14657

[4] Krause et al., "Magnetic particle detection by frequency mixing for immunoassay applications", J. Magn. Magn. Mater. 311, 1, 436 – 444 (2007), DOI: j.jmmm.2006.10.1164

Large single domain iron oxide nanoparticles for extracorporeal heating applications

D. Zahn[1], J. Landers[2], J. Buchwald[1], M. Diegel[3], S. Salamon[2], R. Müller[3], M. Köhler[4], G. Ecke[5], H. Wende[2], S, Dutz[1,3]

[1]*Institute of Biomedical Engineering and Informatics (BMTI), TU Ilmenau, Ilmenau, Germany*
[2] *Faculty of Physics and Center for Nanointegration Duisburg-Essen (CENIDE), University of Duisburg-Essen, Duisburg, Germany*
[3] *Leibniz Institute of Photonic Technology (IPHT), Jena, Germany*
[4] *Jena Center for Soft Matter (JCSM), Friedrich Schiller University Jena, Jena, Germany*
[5] *Institute for Micro- and Nanoelectronics, TU Ilmenau, Ilmenau, Germany*

Introduction

Using iron oxide nanoparticles for hyperthermia treatments is one of the most common applications. Moving from hyperthermia on human patients to technical or biotechnological heating applications, higher field amplitudes and frequencies can be used, enabling the application of particles with larger coercivities (H_C) and thus heating. Therefore, we synthesized large single domain iron oxide particles (LSDP) using the green rust method [1] with varying synthesis conditions. LSDP were characterized in detail regarding their magnetism, structure, heating performance and composition [2].

Methods

LSDP were synthesized under oxygen free conditions using a ferrous chloride solution, NaOH as a precipitation agent and $NaNO_3$ to oxidize the precipitated green rust particles to magnetite within 24 h. The synthesis temperature was varied from 5 to 85 °C in 10 K steps. Resulting particle samples are therefore labelled "S05" to "S85". After several washing steps, the particles were dried at room temperature and the total mass of each sample was determined. To evaluate the particle morphology, size and size distribution, transmission electron microscopy (TEM, FEI Tecnai G2 20, Thermo Fisher Scientific, USA) was used. In more detail their size was determined using X-ray diffraction (XRD, Panalytical X'pert Pro, Malvern Panalytical, The Netherlands) as well as their phase composition. Since non-magnetic parasitic phases were suspected, we used Auger electron spectroscopy (AES, microlab 350, Thermo Fisher Scientific, USA) to determine the chemical composition of the outer layers of the LSDP. Occurrence of iron-containing phases as well as the magnetic alignment behavior was studied in depth by Mössbauer spectroscopy. Basic magnetic parameters were determined with vibrating sample magnetometry (VSM, PPMS Dyna-Cool, Quantum Design, Germany) at 5 and 300 K up to fields of 9 T. Finally, specific absorption rates (SAR) were evaluated using a hyperthermia measurement setup with external field amplitudes of 16, 27 and 55 kA/m at 290 kHz for 1 wt% particles immobilized in agar gel.

Results and discussion

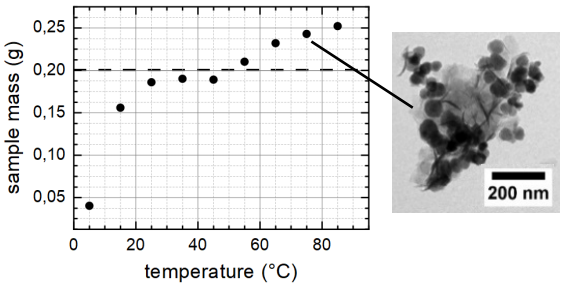

Fig. 1: Mass of the dried particles for each sample depending on synthesis temperature (left) and TEM image for sample S75 (right).

For synthesis temperatures above 50 °C the resulting sample mass exceeds the maximal possible mass if only magnetite and/or maghemite is formed (dashed line in fig. 1). For those samples, TEM images show needle-like structures besides the spherical particles. This implies the formation of phases apart from magnetic iron oxides. Additionally, AES detected sodium in sample S75 (synthesized at 75 °C) besides iron and oxygen.

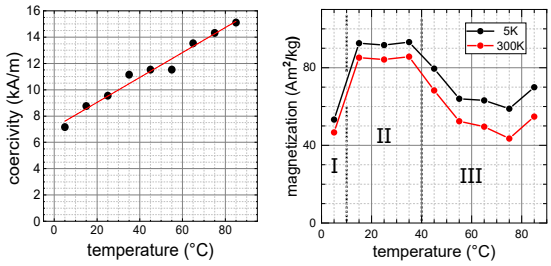

Fig. 2: $H_{C,RT}$ and M_S depending on synthesis temperature.

This presumed non-magnetic phase can be seen in VSM measurements, too. M_S (fig. 2, right) decreases significantly for synthesis temperatures above 45 °C, while an M_S close to the bulk value of magnetite can be reached for 15 to 35 °C (fig. 2, right, segment II). Coercivity (at room temperature) on the other hand increases linearly with increasing temperature (fig. 2, left) and correlates with an increase in particle size (30 to 65 nm, derived from XRD), which proofs the formation of single core particles. H_C values from 7 to 15 kA/m were measured, enabling an open hysteresis loop and thereby an improved heating performance.

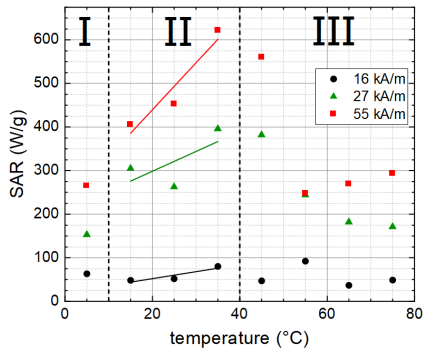

Fig. 3: SAR values depending on synthesis temperature.

Mössbauer spectroscopy measurements identified primarily subspectra characteristics of magnetite-maghemite mixtures, with magnetite being the dominant phase. For samples S45 and higher, an additional subspectral distribution arises, indicating an Fe^{3+}-bearing antiferromagnetic material.
SAR measurements correlate with the magnetic properties (see fig. 3). SAR increases with increasing H_C for the samples with a high M_S (S15 to S35, segment II), reaching 600 W/g and then decreases from S45 onwards because of the growing non-magnetic phase that lowers the M_S.

Conclusion and outlook

We synthesized large single core particles with an increased H_C of 6 to 15 kA/m and mean particle sizes ranging from 30 to 65 nm, depending on the synthesis temperature. From 45 °C onwards, the synthesized particles show a non-magnetic parasitic phase, most likely a Na- and Fe^{3+}-bearing antiferromagnetic phase. This leads to decreasing Ms, decreasing SAR values and an additional subspectrum in Mössbauer spectroscopy measurements.

Acknowledgements

This work was supported by the "Thüringer Innovationszentrum für Medizintechnik-Lösungen" (ThIMEDOP) funded from the Free State of Thuringia (2018 IZN 004), co-financed by the European Union under the European Regional Development Fund (ERDF) as well as by the Federal Ministry for Economic Affairs and Climate Action of Germany in the frame of project "NanoTherMagS (16KN081337)". The TEM facilities of the Jena Center for Soft Matter (JCSM) were established with a grant from the DFG and the European Fonds for Regional Development (EFRE). Funding by the DFG via the CRC/TRR 247 (ID 388390466, Project B2) is acknowledged.

References

[1] Nishio, K. et al. Preparation of size-controlled (30–100nm) magnetite nanoparticles for biomedical applications. Journal of Magnetism and Magnetic Materials 310, 2408-2410, 2007.

[2] Zahn D. et al. Ferrimagnetic Large Single Domain Iron Oxide Nanoparticles for Hyperthermia Applications. Nanomaterials 12/3: 343, 2022.

Adapting magnetic microspheres to medical applications

D. Zahn[1], S. Jung[1], S. Pahlow[2], A. Stanca[1], J. Dellith[2], K. Saatchi[3], U. O. Häfeli[3], S. Dutz[1,2]

[1] *Institut für Biomedizinische Technik und Informatik, Technische Universität Ilmenau, Ilmenau, Germany*
[2] *Leibniz Institute of Photonic Technology - Member of the research alliance "Leibniz Health Technologies", Jena, Germany*
[3] *Faculty of Pharmaceutical Sciences, University of British Columbia, Vancouver, Canada*

Introduction

Polymeric microspheres (MS) are of great interest for a broad range of biomedical applications. In drug delivery approaches they are used as a vehicle for pharmaceutics. By incorporating magnetic nanoparticles (MNP) the resulting magnetic microspheres (MMS) can be used for hyperthermia or temperature triggered drug release and magnetically guided targeting. Last, immobilizing antibodies (AB) on the MMS surface enables immunomagnetic separation, where pathogens are extracted from a specimen magnetically. Each application comes along with specific requirements for the used microspheres. Therefore, we developed a set of MMS whose characteristics regarding their size, MNP content and distribution, drug release and surface functionalization can be customized depending on the application.

Methods

Microspheres were synthesized using an emulsion evaporation method with poly(lactic-co-glycolic)acid (PLGA) or polylactic acid (PLA). The polymer and a drug or MNP as additional components are suspended in an organic solvent and homogenized mechanically in an aqueous polyvinyl alcohol solution to form microdroplets that harden by evaporation of the solvent. To investigate the tunability of MS size, parameters like homogenization speed, time and PVA concentration were varied. MS sizes were determined using a Mastersizer 3000 (Malvern, UK).
Multicore MNP [1] were used for magnetic loading of the MS, resulting in MMS. For this, the MNP need to be suspended in the organic solvent, hence a hydrophobic coating is needed. Therefore, bisphosphonate (BP) was used as a coating material and as a second route, an oleic acid (OA) coating protocol was established.
MNP and MMS were characterized with a vibrating sample magnetometer (MSE-EZ9, Microsense, USA) to determine coercivity (H_C), saturation magnetization (M_S) and the concentration of MNP in the MMS. The specific absorption rate of MMS in water and agar was evaluated using a custom-made hyperthermia measurement setup with an external field of 55 kA/m and 290 kHz.
To evaluate the morphology of the MMS and the MNP distribution, scanning electron microscopy was used (FEI Helios NanoLab G3 UC, USA).
Anticancer drug camptothecin (CPT) was embedded into PLGA-MS using three different lactic to glycolic acid ratios (50:50. 65:35, 75:25). They were kept at 23, 37 and 43 °C in a water bath and the amount of released drug in the supernatant was measured over a period of 24 h using UV-Vis spectroscopy. 43 °C was choosen as a typical hyperthermia temperature.
For the immobilization of antibodies (AB) to the PLA-MMS surface, two routes were evaluated: Protein A and streptavidin-biotin coupling. Bonding of AB to the protein A coated MS was verified using an Enzyme-linked Immunosorbent Assay (ELISA). Streptavidin coating of the MMS was verified using fluorescence measurements (CLARIOstar, BMGLabtech, Germany) of fluorescein-conjugated biotin.

Results and discussion

The emulsion evaporation process results in perfectly spherical solid microspheres and enables mean diameters between 0.6 and 6 µm, with a decrease in size for increasing homogenization velocity and an increasing PVA concentration (see fig. 1).

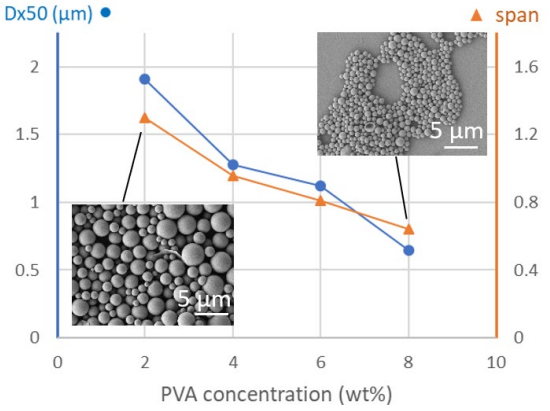

Fig. 1: Influence of PVA concentration on the mean diameter and span of the size distribution of MS.

The OA coating enables a stable suspension with a mean hydrodynamic diameter of 180 – 240 nm of MNP in acetone by creating a coating layer of around 10 wt% related to the total particle mass. Both, MNP with BP and with OA coating were embedded into the MMS leading to the BP ones located on the surface of the spheres, whereas the OA ones are distributed homogeneously within the MMS (see fig. 2).

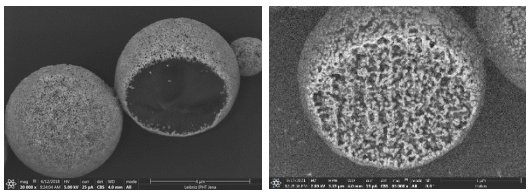

Fig. 2: FIB cross sections of MMS with BP coated MNP (left) and OA coated MNP (right). MNP appear bright.

MMS with 33 wt% OA-MNP show SAR values of around 300 W/g_{MNP} with no significant difference between MMS in water and immobilized in agar. MMS (1 wt% in water) can be heated up to 43 °C within 100 s.

Drug release experiments revealed a burst like release profile with an accelerated release for higher temperatures (see fig. 3) for all used PLGA types as well as a mainly diffusion driven release mechanism indicated by the fast release within hours, whereas degradation of PLGA would take weeks. Human IgG AB were successfully coupled to PLA-MMS via protein A, proven by a qualitative colorimetric reaction between the enzyme conjugated to the AB and a dye. Streptavidin coating of the MMS as a second coupling route was verified with fluorescent biotin as a first step. This enables the binding of biotin-conjugated AB to the streptavidin coated MMS.

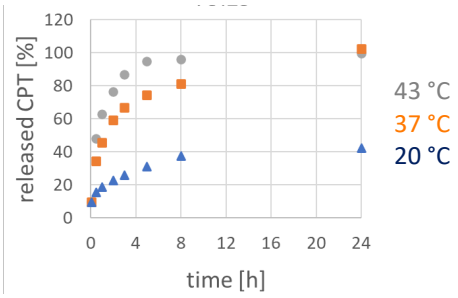

Fig. 3: Drug release for PLGA-MS, L:G=75:25.

Conclusion and outlook

The size of our MS can be tuned between 0.6 and 6 µm with homogenization speed and PVA concentration as the main influencing factors. Oleic acid coated MNP can be incorporated with a concentration of 33 wt% and a homogeneous distribution, enabling magnetic heating of the MMS with an SAR of 300 W/g_{MNP}. Camptothecin as a model drug can be released temperature dependent with a faster release at 43 °C. Antibodys can be immobilized on the MMS via protein A coupling. In ongoing work, coupling via streptavidin-biotin interaction will be finalized. Also, drug release behavior under magnetic heating instead of using a water bath will be studied in more detail. In summary, we are able to modify our MS/MMS synthesis and functionalization, creating a toolbox of MS/MMS for several applications.

Acknowledgements

This work received funding from the Free State of Thuringia (grant 2018 IZN 004), co-financed by the European Union under the European Regional Development Fund (ERDF) and from the Free State of Thuringia within the "SARS-rapid" project (grant 2020FGR0052).

References

[1] Dutz S. et al. 2007, Influence of dextran coating on the magnetic behaviour of iron oxide nanoparticles, J. Magn. Magn. Mater. 311: 51–54.

List of Participants

Christoph Alexiou
Sektion für Experimentelle Onkologie und Nanomedizin (SEON)
Universitätsklinikum Erlangen
Waldstraße 1
91054 Erlangen
Deutschland
Tel.: 91318533142
E-mail: christoph.alexiou@uk-erlangen.de

Sebastian Altmeyer
Department of Physics
Universitat Politecnica de Catalunya
Esteve Terrades 7
8860 Castelldefels
Germany
Tel.: 34692423152
E-mail: sebastian.andreas.altmeyer@upc.edu

Silke Behrens
Institute of Catalysis Research and Technology
Karlsruhe Institute of Technology
Hermann-von-Helmholtz-Platz 1
76344 Eggenstein-Leopoldshafen
Germany
Tel.: 0721 608 26512
E-mail: silke.behrens@kit.edu

Oksana Bilous
Physical Faculty
University of Vienna
Kolingasse 14
1090 Vienna
Austria
Tel.: +380503905997
E-mail: oksana.bilous@univie.ac.at

Dmitry Borin
Institut für Mechatronischen Maschinenbau
TU Dresden
George-Bähr-Str. 3
1062 Dresden
Deutschland
Tel.: 035146332307
E-mail: dmitry.borin@tu-dresden.de

Helmut Brand
Department of Physics
University of Bayreuth
Universitaetsstr. 30
95444 Bayreuth
Germany
Tel.: 0921 55 3331
E-mail: brand@uni-bayreuth.de

Charis Czichy
Lehrstuhl für Magnetofluiddynamik, Mess- und Automatisierungstechnik
TU Dresden
George-Bähr-Straße 3
1069 Dresden
Dtl.
Tel.: +49 (0) 351 463 35157
E-mail: charis.czichy@tu-dresden.de

Silvio Dutz
BMTI
TU Ilmenau
Gustrav-Kirchhoff-Str. 2
98693 Ilmenau
Germany
Tel.: 03677691309
E-mail: silvio.dutz@tu-ilmenau.de

Dietmar Eberbeck
Aug.23
Physikalisch-Technische Bundesanstalt
Abbestraße 2-12
10584 Berlin
Germany
Tel.: 030 34817208
E-mail: dietmar.eberbeck@ptb.de

Alexey Eremin
Nonlinear Phenomena
Otto von Guericke University
Universitaetsplatz 2
39106 Magdeburg
Germany
Tel.: 3916750099
E-mail: alexey.eremin@ovgu.de

Lukas Fischer
Institut für Physik, Theorie der Weichen Materie / Biophysik
Otto-von-Guericke-Universität Magdeburg
Universitätsplatz 01.Jan
39106 Magdeburg
Germany
Tel.: 49-3916751703
E-mail: lukas.fischer@ovgu.de

Philipp Gebhart
Institute of Solid Mechanics
TU Dresden
George-Bähr-Straße 3c
1069 Dresden
Germany
Tel.: +49 351 463-39171
E-mail: philipp.gebhart@tu-dresden.de

Birgit Hankiewicz
Physikalische Chemie
Universität Hamburg
Grindelallee 117
20146 Hamburg
Germany
Tel.: 015781924145
E-mail: birgit.hankiewicz@chemie.uni-hamburg.de

Melissa Hess
Chemie
Universität zu Köln
Luxemburger Str. 116
50939 Köln
Germany
Tel.: 01602369129
E-mail: melissa-hess@gmx.de

Christian Holm
Institute for Computational Physics
University of Stuttgart
Allmandring 02.Jan
70569 Stuttgart
Germany
Tel.: 0711 685 63593
E-mail: holm@icp.uni-stuttgart.de

Darshan Kare Gowda
Professur für Magnetofluiddynamik, Mess- und Automatisierungstechnik
T U Dresden
George-Bähr-Str. 3
1069 Dresden
Germany
Tel.: +49 (0) 351 463 32034
E-mail: darshan.kare_gowda@tu-dresden.de

Karin Koch
Institut für Physikalische Chemie
Universität zu Köln
Greinstraße 4-6
50939 Köln
Deutschland
Tel.: 15785651303
E-mail: karin_ko@gmx.net

Juri Kopp
Physics
University Duisburg-Essen
Lotharstraße 1
47048 Duisburg
Germany
Tel.: +49-(0)203-379-2955
E-mail: juri.kopp@uni-due.de

Michal Kubík
Institute of Machine and Industrial Design
Brno University of Technology
Technická 2
61669 Brno
Czechia
Tel.: 42-0773997941
E-mail: michal.kubik@vutbr.cz

Melvin Küster
Institut für elektrische Messtechnik und Grundlagen der Elektrotechnik und LENA
TU Braunschweig
Hans-Sommer-Straße 66
38106 Braunschweig
Deutschland
Tel.: 0531 391 3854
E-mail: m.kuester@tu-bs.de

Andrey Kuznetsov
Computational and Soft Matter Physics
University of Vienna
Kolingasse 14-16
1090 Wien
Austria
Tel.: 43-68181450163
E-mail: andrey.kuznetsov@univie.ac.at

Ali Lakkis
Experimental physics
Bayreuth University
Brandeburger Strasse 34A
95448 Bayreuth
Germany
Tel.: 00491731728566
E-mail: Ali.Lakkis@uni-bayreuth.de

Joachim Landers
Physik
Universität Duisburg-Essen
Lotharstr. 1
47057 Duisburg
Germany
Tel.: 0203-3792384
E-mail: joachim.landers@uni-due.de

Adrian Lange
Lehrstuhl für Magnetofluiddynamik,
Mess- und Automatisierungstechnik
TU Dresden, Institut für Mechtronischen
Maschinenbau
George-Bähr-Straße 3a
1062 Dresden
BRD
Tel.: 0049-351-46334703
E-mail: adrian.lange@tu-dresden.de

Michael Lentze
Engineering Devision
DFG
Kennedyallee 40
53170 Bonn
Germany
Tel.: +49 228 885 2449
E-mail: michael.lentze@dfg.de

Frank Ludwig
Institut für Elektrische Messtechnik und
Grundlagen der Elektrotechnik
TU Braunschweig
Hans-Sommer-Str. 66
38106 Braunschweig
Germany
Tel.: 0531-3913863
E-mail: f.ludwig@tu-bs.de

Stefan Lyer
Sektion für experimentelle Onkologie und
Nanomedizin (SEON)
Universitätsklinikum Erlangen
Glückstraße 10a
91054 Erlangen
Deutschland
Tel.: 09131 85 33142
E-mail: stefan.lyer@uk-erlangen.de

Stefan G. Mayr
Biokompatible und Bioaktive Oberflächen
/ Oberflächenphysik
IOM Leipzig / Universität Leipzig
Permoserstr. 15
4318 Leipzig
Germany
Tel.: +49 341 / 235-3368
E-mail: stefan.mayr@iom-leipzig.de

Andreas Menzel
Theorie der Weichen Materie / Biophysik
Otto-von-Guericke-Universität
Magdeburg
Universitätsplatz 2
39106 Magdeburg
Deutschland
Tel.: 0391 67 57490
E-mail: a.menzel@ovgu.de

Hajnalka Nádasi
Department of Nonlinear Phenomena
Otto von Guericke University
Univeritätsplatz 2
39106 Magdeburg
Germany
Tel.: 03916750098
E-mail: hajnalka.nadasi@ovgu.de

Stefan Odenbach
Magnetofluiddynamik, Mess- und
Automatisierungstechnik
TU Dresden
George-Bähr-Str. 3
1069 Dresden
Germany
Tel.: 0351-46332062
E-mail: stefan.odenbach@tu-dresden.de

Felix Pfister
HNO - Sektion für Experimentelle
Onkologie und Nanomedizin (SEON)
Universitätsklinikum Erlangen
Glückstraße 10a
91054 Erlangen
Deutschland
Tel.: +49/9131/85-43928
E-mail: felix.pfister@gmx.net

Surojit Ranoo
Department für Chemie
Universität zu Köln
Greinstraße 4-6
50939 Köln
Germany
Tel.: +49 221 470 5472
E-mail: sranoo@uni-koeln.de

Marius Reiche
Technische Mechanik
Technische Universität Ilmenau
Ehrenbergstraße 29
98693 Ilmenau
Deutschland
Tel.: 03677 / 69-1884
E-mail: marius.reiche@tu-ilmenau.de

Benoît Rhein
Chemistry Department
Universität zu Köln
Greinstraße 04.Jun
50939 Cologne
Germany
Tel.: 0221 470 4459
E-mail: brhein@uni-koeln.de

Reinhard Richter
Experimentalphysik 5
Universität Bayreuth
Gotthelfstrasse 2
95447 Bayreuth
Germany
Tel.: 0921-553311
E-mail: reinhard.richter@uni-
bayreuth.de

Margaret Rosenberg
Fakultät für Physik
Universität Wien
Kolingasse 14-16
1090 Wien
Österreich
Tel.: 43-6508084280
E-mail: margaret.rosenberg@univie.ac.at

Annette Schmidt
Chemistry Department
Universität zu Köln
Greinstr. 4 - 6
50939 Köln
Germany
Tel.: +49 221 4705410
E-mail: annette.schmidt@uni-koeln.de

Thilo Viereck
Inst. f. Elektr. Messtechnik (EMG)
TU Braunschweig
Hans-Sommer-Straße 66
38106 Braunschweig
Germany
Tel.: 0531 391 3860
E-mail: t.viereck@tu-braunschweig.de

Thomas Wallmersperger
Maschinenwesen
IFKM/TU Dresden
George-Bähr-Str. 3c
1069 Dresden
Germany
Tel.: +49 351 463-37013
E-mail: thomas.wallmersperger@tu-
dresden.de

Rudolf Weeber
Institute for Computational Physics
University of Stuttgart
Allmandring 3
70569 Stuttgart
Germany
Tel.: 0711 685-67609
E-mail: rudolf.weeber@icp.uni-
stuttgart.de

Maria Weißpflog
Institute of Physical Chemistry
University of Hamburg
Grindelallee 117
20146 Hamburg
Germany
Tel.: +49 40 42838 3428
E-mail: maria.weisspflog@chemie.uni-
hamburg.de

Florian Wolgast
Institut für elektrische Messtechnik und
Grundlagen der Elektrotechnik
TU Braunschweig
Hans-Sommer-Straße 66
38106 Braunschweig
Deutschland
Tel.: +49 531 391 3876
E-mail: f.wolgast@tu-bs.de

Diana Zahn
Institut für Biomedizinische Technik und
Informatik
TU Ilmenau
Gustav-Kirchhoff Str. 2
98693 Ilmenau
Deutschland
Tel.: 03677691970
E-mail: diana.zahn@tu-ilmenau.de